Distances and metallicities for 17 Local Group galaxies

A. W. McConnachie,[1]⋆ M. J. Irwin,[1] A. M. N. Ferguson,[2] R. A. Ibata,[3] G. F. Lewis[4] and N. Tanvir[5]

[1]*Institute of Astronomy, Madingley Road, Cambridge CB3 0HA*
[2]*Max-Planck-Institut für Astrophysik, Karl-Schwarzschild-Str. 1, Postfach 1317, D-85741 Garching, Germany*
[3]*Observatoire de Strasbourg, 11, rue de l'Universite, F-67000, Strasbourg, France*
[4]*Institute of Astronomy, School of Physics, A29, University of Sydney, NSW 2006, Australia*
[5]*Physical Sciences, University of Hertfordshire, Hatfield AL10 9AB*

ABSTRACT

We have obtained Johnson *V* and Gunn *i* photometry for a large number of Local Group galaxies using the Isaac Newton Telescope Wide Field Camera (INT WFC). The majority of these galaxies are members of the M31 subgroup and the observations are deep enough to study the top few magnitudes of the red giant branch in each system. We previously measured the location of the tip of the red giant branch (TRGB) for Andromeda I, Andromeda II and M33 to within systematic uncertainties of typically <0.05 mag. As the TRGB acts as a standard candle in old, metal-poor stellar populations, we were able to derive distances to each of these galaxies. Here we derive TRGB distances to the giant spiral galaxy M31 and 13 additional dwarf galaxies – NGC 205, 185, 147, Pegasus, WLM, LGS3, Cetus, Aquarius, And III, V, VI, VII and the newly discovered dwarf spheroidal And IX. The observations for each of the dwarf galaxies were intentionally taken in photometric conditions. In addition to the distances, we also self-consistently derive the median metallicity of each system from the colour of their red giant branches. This allows us to take into account the small metallicity variation of the absolute *I* magnitude of the TRGB. The homogeneous nature of our data and the identical analysis applied to each of the 17 Local Group galaxies ensures that these estimates form a reliable set of distance and metallicity determinations that are ideal for comparative studies of Local Group galaxy properties.

Key words: galaxies: general – Local Group – galaxies: stellar content.

1 INTRODUCTION

The Local Group is home to some 35 galaxies, the majority of which are suspected to be satellites of the two most massive bodies, the Galaxy and M31 (for recent reviews, see Mateo 1998; Lynden-Bell 1999; van den Bergh 1999). Many of the dwarfs, such as M32, have been known about for decades, while others, such as And V, VI, VII and IX are recent discoveries (Armandroff, Davies & Jacoby 1998; Armandroff, Jacoby & Davies 1999; Karachentsev & Karachentseva 1999; Zucker et al. 2004). As the discovery of And IX by Zucker et al. (2004) demonstrates, it is unlikely that even now we have a full inventory of the Local Group, and no doubt some faint bodies still await discovery. Interest in Local Group galaxies stems from their proximity and representative nature, since they are relatively easily resolved and include examples over a wide range of luminosities.

With so many galaxies known in the Local Group it has become possible to conduct comparative studies of the different population

types such as the dwarf irregulars and dwarf spheroidals. However, accurate studies of stellar populations require accurate knowledge of the distance to each galaxy, and this becomes significantly more important when populations in different galaxies are to be compared. The distances to the nearby satellites of the Milky Way are believed to be known to reasonable accuracy and are based on a variety of methods. However, this is not always the case for the more distant Local Group galaxies, such as the satellites of M31. Furthermore, the majority of distance determinations to these galaxies have been conducted as independent studies by different groups. It is nevertheless advantageous to acquire a homogeneous set of distance determinations. This then removes systematic uncertainties that may exist between measurements that could be due to the data aquisition/reduction process, the standard candle employed, and the algorithm that is applied. Reliable relative distances to the galaxies can then be obtained, and provides much of the motivation behind the work presented in this paper.

All of the Local Group galaxies contain a significant population of old, relatively metal-poor stars (Population II). For M31 and

⋆E-mail: alan@ast.cam.ac.uk

© 2004 RAS

the Galaxy, these stars are found predominantly in the stellar halo, while for the dwarfs, Population II stars tend to be the dominant component. A lack of Cepheid variables in this population means that in order to estimate distances to them other indicators have to be used. One obvious candidate is based on the tip of the red giant branch (TRGB). This point in stellar evolution marks the onset of core helium burning in red giant branch (RGB) stars and observation and theory show it to occur at a relatively constant *I*-band magnitude (e.g. Da Costa & Armandroff 1990; Salaris & Cassisi 1997). Barker, Sarajedini & Harris (2004) have recently conducted a detailed study of the reliability of the TRGB as a distance indicator for stellar populations with a variety of star formation histories and find that it is reliable for any system which is not dominated by a metal-rich population ([Fe/H] > -0.3) or a population with a substantial young ($\lesssim$1.7 Gyr) component. This makes it ideal for calculating distances in the Local Group.

Lee, Freedman & Madore (1993b) were influential in developing a quantitative technique, based upon a Sobel edge-detection algorithm, for detecting the location of the TRGB in a photometric data set. It was later adapted and refined by Sakai, Madore & Freedman (1996) and, more recently, Méndez et al. (2002) who also developed a maximum-likelihood approach to estimate the TRGB location. Edge-detection algorithms essentially assume that the luminosity function in the region of the tip are step-like, and their simplest application looks for the largest absolute change in star counts between neighbouring bins in the luminosity function. As such, they can be easily affected by the noise features which are often prevalent in real luminosity functions on which TRGB analyses are to be conducted.

In a previous paper (McConnachie et al. 2004a, hereafter Paper I), we developed a new technique to allow for the accurate determination of the TRGB as represented in a photometric data set. We advocated the use of Wide Field Cameras for such a study as this maximizes the number of stars that contribute to the luminosity function, decreasing the effects of Poisson noise on the measurement and ensuring that a fair sample of the brightest RGB stars are present. In Paper I we also introduced, tested and implemented a new algorithm for TRGB determination which uses a data-adaptive slope to fit the 'luminosity probability distribution' (LPD) in the region of the tip and hence derive a distance modulus for the system. The LPD is given by

$$\wp\,(m) = \sum_{i=1}^{N_\star} \frac{1}{\sqrt{2\pi}\sigma_i} \exp\left[-\frac{(m_i - m)^2}{2\sigma_i}\right], \tag{1}$$

where m_i and σ_i are the magnitude and photometric error of the *i*th star from a sample of $N_\star$. This technique was shown to have systematic uncertainties usually of order <0.05 mag. We went on to calculate the distances, as derived from data taken with the Isaac Newton Telescope Wide Field Camera (INT WFC), to the dwarf galaxies And I and II, and the spiral galaxy M33. The reader is referred to this paper, and references therein, for a discussion of the practicalities involved with this technique.

In this paper, we significantly extend the number of Local Group galaxies for which we have measured locations of the TRGB and distances, based on a large homogeneous photometric database of Local Group galaxies. These data have been taken with the INT WFC, a four-chip EEV 4K × 2K CCD mosaic camera with a ∼0.29 deg^2 field of view (Walton et al. 2001). Over the past three years we have been using this instrument in conjunction with the Canada–France–Hawaii 12K Camera to conduct a photometric survey of M31 (Ibata et al. 2001; Ferguson et al. 2002; McConnachie

et al. 2003; Irwin et al., in preparation), which is now complete over an area of 40 deg^2. We have also presented photometry for M33, and And I and II (Paper I; see also Ferguson et al., in preparation), and here we present colour–magnitude diagrams (CMDs), metallicity information and distance determinations to And III, V, VI, VII, IX, LGS3, Cetus, WLM, Pegasus, Aquarius, NGC 147, 185, 205 and M31. These galaxies constitute the majority of Local Group members visible from the northern hemisphere. M32 is not included in this list due to severe crowding problems and its awkward projected location close to the centre of M31. Our data for IC 10 is likewise not presented here as the close proximity of this object to the Galactic plane causes a serious amount of differential reddening which complicates its analysis. For the rest, the resulting set of homogeneous distance estimates is the largest that has been measured for the Local Group: the data for each galaxy were taken using the same telescope and the same instrument, through the same filters for similar exposure times.

The data for the dwarf galaxies were taken in conjunction with the main M31 and M33 surveys. Observations for each dwarf galaxy were restricted to photometric conditions simplifying cross-calibration of all the data to the same photometric system. All data taken were then reduced and calibrated in exactly the same way with the same pipeline processing (Irwin & Lewis 2001). The subsequent analysis for each galaxy was also identical, with the same algorithm applied to each to derive the distance estimates. As such, differential systematic errors are minimized and the entire data set is thus ideal for comparative studies of these galaxies.

Section 2 provides an overview of our photometry, discusses the reddening estimates, the assumed absolute *I* magnitude of the TRGB, the metallicity determination and how we deal with foreground and background contamination. In Section 3 we briefly review the current knowledge of the stellar content of each of the galaxies and calculate the median metallicity and distance to each from the INT WFC data. We finish in Section 4 with a discussion of our results and a comparison to previous work.

2 PRELIMINARIES

2.1 Photometry

All the photometry for the dwarf galaxies analysed in this paper consists of a single targeted WFC pointing, with the exception of And III, which fell across two pointings, as part of the M31 survey. The data for the isolated dwarf galaxies were all systematically taken in photometric conditions as part of two separate M31 and M33 survey runs in 2003 August and September. As for the main surveys, the INT WFC Gunn i(i') and Johnson V(V') passbands were used. Exposure times were 800–1000 s per passband and allowed us to probe down to magnitudes of 23.5 mag in i' and 24.5 mag in V'(S/N $\simeq$ 5). Depending upon the galaxy, this is usually sufficient to detect individual RGB stars to an absolute magnitude of $V' \simeq$ 0 and main-sequence stars to $V' \simeq -1$. For the subsequent analysis, we have converted our data to the Landolt equivalent passbands V and I (Landolt 1992). The transformations required are $I = i' - 0.101 \times (V - I)$ and $V = V' + 0.005 \times (V - I)$. These transformations have been derived by comparison with observations of several Landolt standard fields.[1] The standard INT Wide Field Survey (WFS) pipeline, supplied by the Cambridge Astronomical Survey Unit (Irwin & Lewis 2001), was used to process all of the on-target

---

[1] http://www.ast.cam.ac.uk/∼wfcsur/colours.php

data plus calibration frames, as was the case for Paper I. Our final uncertainty in the distances we derive includes the average rms photometric error in the region of the TRGB, which is typically 0.02 mag at $I \simeq 20.5$ mag, and the average photometric zero-point calibration error, also of order 0.02 mag.

Objects are classified independently in each passband based on their overall morphological properties, specifically their ellipticity as derived from intensity-weighted second moments and the curve-of-growth of their flux distribution (Irwin et al. 2004). Measures from these are combined to produce a normalized N(0,1) statistic which compares the likeness of each object to the well-defined stellar locus visible on each frame. Stellar objects are chosen to lie within 2σ or 3σ of this locus depending on the desired trade-off between completeness and contamination from non-stellar objects (usually compact galaxies or spurious images). For the purposes of this study, we generally make use of all objects which lie within 3σ of the stellar locus. For situations in which many sources are available to us, we use the more stringent 2σ limit. At faint magnitudes, typically within 1–2 mag of the frame limit (depending on seeing), the stellar locus is vulnerable to contamination by distant compact galaxies. However, this has little effect here as we are mainly concerned with the relatively bright stars near the TRGB.

2.2 Foreground contamination

Each red giant branch luminosity function/LPD is statistically corrected for foreground stars, as was the case in Paper I. Except for M31 and NGC 205, this is done in a standard way. In constructing the CMD for the galaxy, we try to use stars within $\sim 0.2°$ of the centre of the galaxy, i.e. approximately 40 per cent of the area of the INT WFC field is used. Allowing for foreground stars, this means that we generally use somewhere in the region of 50–100 per cent of the stars that belong to the dwarf galaxy that we have detected. For some of the smaller, fainter objects, such as And V or Aquarius, we have been forced to use a smaller area to detect more clearly the RGB over and above the Galactic foreground. However, even in these situations we are still sampling all the bright RGB stars within ~ 5 core radii (r_c). Generally, the outer regions of each INT WFC pointing are used in constructing a reference luminosity function. This is scaled to the actual luminosity function either by matching the number of brighter foreground stars in each zone or by simply computing the area ratio used. In the case of M31 and NGC 205 we adopted a different strategy making use of the larger area survey available; details of this are given in the appropriate section. Additionally, the TRGB location in M33 has been rederived making use of a local foreground correction in exactly the same way as will be described for M31, and using only objects lying within 2σ of the stellar locus. The former alteration causes a 0.03 mag difference with the result presented in Paper I (see Tables 1 and 2).

2.3 Reddening corrections

All reddening corrections used in this paper are taken from Schlegel, Finkbeiner & Davis (1998). These authors conducted an all-sky survey of infrared dust emission and used this to calculate the reddening, $E(B - V)$, across the sky to within an uncertainty of ~ 16 per cent. We have also included the effects of this error in our final error estimation. The extinction in the I-band is calculated by the relationship given in the same paper, $A_I = 1.94 E(B - V)$. We note that Arce & Goodman (1999) and Bonifacio, Monai & Beers (2000) have suggested that the Schlegel maps may overestimate the reddening values in areas where the colour excess is larger than $E(B - V) \simeq 0.1$ mag. We do not consider this effect here for the sake of homogeneity, and if real it will affect very few of our results, none of them significantly (<0.035 mag). All adopted reddening values are listed in Table 1 to allow the distance moduli to be recalculated should later work produce revised estimates for the reddening.

2.4 Absolute I magnitude of the TRGB

In Paper I, we adopted the blanket value of 4.04 ± 0.05 mag as the absolute I magnitude of the TRGB, based upon the value given by Bellazzini, Ferraro & Pancino (2001). These authors calculated $M_I^{\mathrm{TRGB}} = -4.04 \pm 0.12$ mag at $[\mathrm{Fe/H}] \sim -1.7$ by analysis of the red giant branch of Omega Centauri. The large uncertainty in this value comes primarily from the uncertainty in the distance modulus to ω Cen. The value they adopted for this was derived by Thompson et al. (2001) by observations of a detached eclipsing binary, for which a value of $(m - M)_\mathrm{o} = 13.65 \pm 0.11$ was calculated. The value of M_I^{TRGB} calculated by Bellazzini et al. (2001) is in excellent agreement with that derived by other means, and the quoted uncertainty is somewhat conservative. For this reason we adopted the smaller uncertainty of 0.05 mag, but noted that it is possible for the entire scale to shift by some larger amount, affecting all our distance estimates in the same fashion.

In this paper, we now also take into account the slight variation that M_I^{TRGB} displays with metallicity (e.g. Bellazzini et al. 2001, 2004). This is generally a small effect; however, the spread in metallicity shown by the galaxies that we are analysing necessitates that we take this effect into account. The most recent empirical calibration of this is by Bellazzini et al. (2004) who fit the following relationship:

$$M_I^{\mathrm{TRGB}} = 0.258 \left[\frac{\mathrm{M}}{\mathrm{H}}\right]^2 + 0.676 \left[\frac{\mathrm{M}}{\mathrm{H}}\right] - 3.629$$
$$= f\left(\left[\frac{\mathrm{M}}{\mathrm{H}}\right]\right). \qquad (2)$$

At intermediate metallicities ($[\mathrm{M/H}] \sim -1.5$) this relation predicts values of M_I^{TRGB} similar to the 'standard' value of ~ -4.04 mag. However, at very low metallicities (e.g. LGS3, Aquarius; $[\mathrm{M/H}] < -2$) the values predicted are substantially fainter ($M_I^{\mathrm{TRGB}} \sim -3.95$ mag) than normally assumed. It is unclear at this time whether such faint values are realistic or what the physical explanation for the reduced luminosity would be. Although line blanketing effects lead to a reduction in the I-band luminosity at high metallicity, an equivalent dimming effect has not been reported in the literature for low metallicity. Our own work on M31 suggests there is no strong evidence to suggest that M_I^{TRGB} becomes fainter at low metallicity and we find that the behaviour of M_I^{TRGB} with metallicity is well approximated by the evolutionary tracks of VandenBerg et al. (2000) (McConnachie et al. 2003). Since the dimming may well be an artefact of the empirical calibration used, for systems more metal-poor than ω Cen, we adopt $M_I^{\mathrm{TRGB}} = \min\{-4.04, f([\mathrm{M/H}])\}$. Although this modified calibration is still ad hoc, it nevertheless prevents physically implausible levels of dimming at low metallicity.

In Tables 1 and 2 we provide the reader with all the necessary information to recalculate the distance moduli should later work produce improved calibrations. The distances to Andromeda I, Andromeda II and M33, which were originally calculated in Paper I, have been recalculated to account for this small metallicity dependency. The results for these galaxies are also listed in Tables 1 and 2 along with the 14 galaxies examined here.

Table 1. The position, adopted reddening, median metallicity and adopted value of M_I^{TRGB} for each of the galaxies in our data set. The reddening values have been taken from the maps produced by Schlegel et al. (1998) and are related to the extinction in the *I*-band via $A_I = 1.94\,E(B-V)$. The median metallicity has been calculated for each system using the evolutionary tracks produced by VandenBerg et al. (2000) and is calculated such that it is consistent with the TRGB measurement. Two values are quoted as we consider both $\alpha = 0.0$ and $\alpha = 0.3$. The implied value of M_I^{TRGB} has been calculated for each case using the modified calibration of Bellazzini et al. (2004) (see Section 2.4). There is little difference in M_I^{TRGB} between the $\alpha = 0.0$ and $\alpha = 0.3$ cases. LGS3 and Aquarius are at least as metal-poor as our most metal-poor evolutionary track. The three galaxies analysed in Paper I are included in this table, and their final distance estimates have been revised accordingly.

	RA (J2000)	Dec. (J2000)	$E(B-V)$	[M/H] $\alpha = 0.0$	$\alpha = 0.3$	M_I^{TRGB} $\alpha = 0.0$	$\alpha = 0.3$	Adopted
M31	$00^{\mathrm{h}}\,42^{\mathrm{m}}\,44\overset{\mathrm{s}}{.}3$	$+41°\ 16'\ 09''$	0.060	-0.6	-0.5	–	–	-4.05^a
M33	$01^{\mathrm{h}}\,33^{\mathrm{m}}\,50\overset{\mathrm{s}}{.}9$	$+30°\ 39'\ 36''$	0.042	-0.8	-0.7	–	–	-4.05^a
NGC 205	$0^{\mathrm{h}}\,40^{\mathrm{m}}\,22\overset{\mathrm{s}}{.}1$	$+41°\ 41'\ 07''$	0.062	-0.8	-0.7	–	–	-4.05^a
NGC 185	$00^{\mathrm{h}}\,38^{\mathrm{m}}\,58\overset{\mathrm{s}}{.}0$	$+48°\ 20'\ 15''$	0.179	-1.2	-1.1	-4.07	-4.06	-4.065
NGC 147	$00^{\mathrm{h}}\,33^{\mathrm{m}}\,12\overset{\mathrm{s}}{.}1$	$+48°\ 30'\ 32''$	0.175	-1.1	-1.0	-4.06	-4.05	-4.055
Pegasus	$23^{\mathrm{h}}\,28^{\mathrm{m}}\,36\overset{\mathrm{s}}{.}2$	$+14°\ 44'\ 35''$	0.064	-1.4	-1.2	-4.07	-4.07	-4.07
WLM	$00^{\mathrm{h}}\,01^{\mathrm{m}}\,58\overset{\mathrm{s}}{.}1$	$-15°\ 27'\ 39''$	0.035	-1.5	-1.4	-4.06	-4.07	-4.065
LGS3	$01^{\mathrm{h}}\,03^{\mathrm{m}}\,52\overset{\mathrm{s}}{.}9$	$+21°\ 53'\ 05''$	0.042	$\lesssim -2.3$	$\lesssim -2.0$	-4.04	-4.04	-4.04
Cetus	$00^{\mathrm{h}}\,26^{\mathrm{m}}\,11\overset{\mathrm{s}}{.}0$	$-11°\ 02'\ 40''$	0.029	-1.6	-1.5	-4.05	-4.06	-4.055
And I	$00^{\mathrm{h}}\,45^{\mathrm{m}}\,39\overset{\mathrm{s}}{.}8$	$+38°\ 02'\ 28''$	0.056	-1.4	-1.3	-4.07	-4.07	-4.07
And II	$01^{\mathrm{h}}\,16^{\mathrm{m}}\,29\overset{\mathrm{s}}{.}8$	$+33°\ 25'\ 09''$	0.063	-1.5	-1.4	-4.06	-4.07	-4.065
And III	$00^{\mathrm{h}}\,35^{\mathrm{m}}\,33\overset{\mathrm{s}}{.}8$	$+36°\ 29'\ 52''$	0.058	-1.7	-1.6	-4.04	-4.05	-4.045
And V	$01^{\mathrm{h}}\,10^{\mathrm{m}}\,17\overset{\mathrm{s}}{.}1$	$+47°\ 37'\ 41''$	0.124	-1.6	-1.5	-4.05	-4.06	-4.055
And VI	$23^{\mathrm{h}}\,51^{\mathrm{m}}\,46\overset{\mathrm{s}}{.}3$	$+24°\ 34'\ 57''$	0.065	-1.5	-1.3	-4.06	-4.07	-4.065
And VII	$23^{\mathrm{h}}\,26^{\mathrm{m}}\,31\overset{\mathrm{s}}{.}0$	$+50°\ 41'\ 31''$	0.199	-1.4	-1.3	-4.07	-4.07	-4.07
And IX	$00^{\mathrm{h}}\,52^{\mathrm{m}}\,52\overset{\mathrm{s}}{.}8$	$+43°\ 12'\ 00''$	0.076	-1.5	-1.4	-4.06	-4.07	-4.065
Aquarius	$20^{\mathrm{h}}\,46^{\mathrm{m}}\,51\overset{\mathrm{s}}{.}8$	$-12°\ 50'\ 53''$	0.052	$\lesssim -2.3$	$\lesssim -2.0$	-4.04	-4.04	-4.04

^{a}Calculated using the representative metallicity of the RGB stars contained within the strip used in the TRGB measurement. Due to the width of the RGB in M31, M33 and NGC 205, this does not correspond to the median metallicity of the RGB in these cases (see Fig. 1 for M31, fig. 5 in Paper I for M33, and Fig. 2 for NGC 205). In each of these cases the representative metallicity is [M/H]~ -1.

2.4.1 Calculating M/H

In order to maintain internal consistency and also as an independent metallicity measure, we choose not to use metallicity estimates for each system from the literature but instead calculate the metallicity of each system from the locus of the RGB in the INT WFC data. VandenBerg et al. (2000) produced an extensive set of theoretical evolutionary tracks that trace stellar evolution up to the point of core helium ignition. A metallicity distribution function (MDF) can be readily constructed for each system using these tracks by making the plausible assumptions that the majority population seen on the putative RGB is composed of first ascent giants, and has an age greater than 2 Gyr. A full description of the technique used to construct the MDFs and an analysis of the metallicity information for each galaxy will be presented elsewhere (McConnachie, in preparation) together with a detailed study of the metallicity variation in and around M31. It should be noted that our technique is essentially the same as that employed by numerous other authors (see, for example Durrell, Harris & Pritchet 2001, 2004;

Bellazzini et al. 2003) and so we give only a brief description below.

The evolutionary tracks are first shifted in colour–magnitude space so that they lie at the reddening and (approximate) distance of the system we wish to analyse. For each star in the top two magnitudes of the RGB we then calculate its metallicity using a bilinear interpolation from the evolutionary tracks that lie either side of the star. A MDF is then obtained by constructing a histogram of the resulting metallicity estimates. The foreground is removed by constructing a suitable reference field and subtracting it from the galaxy MDF. However, since M_I^{TRGB} also depends on metallicity then so does the distance against which the tracks are registered. We thus need to iterate towards a final solution for the metallicity and distance modulus using the newly estimated median metallicity for each system, to update the value of M_I^{TRGB} and then repeating the procedure until it converges. The accuracy of this technique is estimated to be ± 0.1–0.2 dex.

This process is conducted twice for each system, using tracks with no α-element enhancement and tracks with an α-element

Table 2. The measured value of the TRGB, implied distance modulus and distance to each galaxy analysed, along with previous estimates. The latter are representative only and do not form an exhaustive list. The distance estimates to the galaxies analysed in Paper I have been revised in accordance with the methods presented in this paper. In addition, the TRGB location for M33 has been rederived using a local foreground correction in the same way as for M31 and using only objects lying within 2σ of the stellar locus.

	I_{TRGB}	$(m-M)_\circ$	D (kpc)		ΔD (kpc)	Previous estimates	References
M31	20.54 ± 0.03	24.47 ± 0.07	785	$\pm$	25	794 ± 37 kpc	Brown et al. (2004)
						791 ± 40 kpc	Joshi et al. (2003)
						783 ± 43 kpc	Durrell et al. (2001)
						773 ± 36 kpc	Freedman & Madore (1990)
M33	20.57 ± 0.03	24.54 ± 0.06	809	$\pm$	24	855 ± 60 kpc	Galleti, Bellazzini & Ferraro (2004)
						867 ± 28 kpc	Tiede, Sarajedini & Barker (2004)
						802 ± 51 kpc	Lee et al. (2002)
						916 ± 55 kpc	Kim et al. (2002)
NGC 205	20.65 ± 0.03	24.58 ± 0.07	824	$\pm$	27	809 ± 80 kpc	Salaris & Cassisi (1998)
						851 ± 98 kpc	Saha, Hoessel & Krist (1992)
						863 ± 139 kpc	Ciardullo et al. (1989)
						724 ± 67 kpc	Mould et al. (1984)
NGC 185	20.23 ± 0.03	23.95 ± 0.09	616	$\pm$	26	617 ± 28 kpc	Martínez-Delgado & Aparicio (1998)
						620 ± 60 kpc	Lee et al. (1993a)
NGC 147	20.43 ± 0.04	24.15 ± 0.09	675	$\pm$	27	755 ± 17 kpc	Han et al. (1997)
						608 ± 70 kpc	Saha, Hoessel & Mossman (1990)
						630 ± 50 kpc	Mould, Kristian & Da Costa (1983)
Pegasus	20.87 ± 0.03	24.82 ± 0.07	919	$\pm$	30	760 ± 100 kpc	Gallagher et al. (1998)
						955 ± 44 kpc	Aparicio (1994)
						1.7 ± 0.23 Mpc	Hoessel & Mould (1982)
WLM	20.85 ± 0.05	24.85 ± 0.08	932	$\pm$	33	977 ± 58 kpc	Rejkuba et al. (2000)
						891 ± 41 kpc	Minniti & Zijlstra (1997)
LGS3	20.47 ± 0.03	24.43 ± 0.07	769	$\pm$	23	770 ± 70 kpc	Aparicio et al. (1997)
						810 ± 80 kpc	Lee (1995)
Cetus	20.39 ± 0.03	24.39 ± 0.07	755	$\pm$	23	780 ± 50	Sarajedini et al. (2002)
						775 ± 50	Whiting et al. (1999)
And I	20.40 ± 0.03	24.36 ± 0.07	745	$\pm$	24	810 ± 30 kpc	Da Costa et al. (1996)
						790 ± 60 kpc	Mould & Kristian (1990)
And II	20.13 ± 0.02	24.07 ± 0.06	652	$\pm$	18	665 ± 20 kpc	Pritzl et al. (2004)
						680 ± 20 kpc	Da Costa et al. (2000)
						583^{+124}_{-103} kpc	Koenig et al. (1993)
And III	20.44 ± 0.04	24.37 ± 0.07	749	$\pm$	24	752 ± 21 kpc	Da Costa et al. (2002)
						758 ± 70 kpc	Armandroff et al. (1993)
And V	20.63 ± 0.04	24.44 ± 0.08	774	$\pm$	28	810 ± 45 kpc	Armandroff et al. (1998)
And VI	20.53 ± 0.04	24.47 ± 0.07	783	$\pm$	25	815 ± 25 kpc	Pritzl et al. (2002)
						830 ± 80 kpc	Grebel & Guhathakurta (1999)
						820 ± 94 kpc	Tikhonov & Karachentsev (1999)
						775 ± 35 kpc	Armandroff et al. (1999)
						794 ± 73 kpc	Hopp et al. (1999)
And VII	20.73 ± 0.05	24.41 ± 0.10	763	$\pm$	35	760 ± 70 kpc	Grebel & Guhathakurta (1999)
						708 ± 81 kpc	Tikhonov & Karachentsev (1999)
And IX	20.50 ± 0.03	24.42 ± 0.07	765	$\pm$	24	790 ± 70 kpc	Zucker et al. (2004)
Aquarius	21.21 ± 0.04	25.15 ± 0.08	1071	$\pm$	39	950 ± 50 kpc	Lee et al. (1999)
						~ 4 Mpc	Greggio et al. 1993

enhancement of 0.3. Although there is little evidence to suggest that any of the dwarfs have an α enhancement, we do not want to misinterpret a lack of evidence as evidence for a lack. It transpires that the median value of [M/H] is relatively insensitive to the α-element abundance assumed, and the implied value of M_I^{TRGB} changes by, at most, a few hundredths of a magnitude. This has a negligible effect on the distance that we would calculate and we are thus able to derive a unique distance to each galaxy.

Although this procedure was adopted for the majority of the galaxies studied, the much broader metallicity spread for M31 and NGC 205 (and M33) required a slight variant on this scheme. Generally, the strip of stars used in calculating the position of the TRGB spans approximately the entire RGB, and thus the median metallicity of the RGB is essentially the representative metallicity of the tip. For the three cases mentioned here, however, the strip used to calculate the position of the tip is substantially narrower than the RGB, and so the representative metallicity of the tip is *not* well approximated by the median metallicity of the RGB. In these cases, we instead use the metallicity of the evolutionary track that best matches the position of the chosen analysis strip. Without this restriction the much larger spread in metallicities on the metal-rich side for these galaxies blurs out the position of the tip and also systematically lowers M_I^{TRGB}. Furthermore, by restricting the range in metallicity used we also reduce the dependence on the empirical relationship in equation (2). For completeness, we still include the calculated RGB median metallicities for these systems in Table 1.

3 TRGB DISTANCE DETERMINATIONS

Figs 1–14 show the CMDs for each galaxy (left panel). The luminosity function (histogram in upper right panel) and the LPD on which our algorithm is applied (offset curve in upper right panel) are constructed only from stars which are limited by the dashed lines in the CMD, to reduce contamination from other stellar populations. An arrow shows the measured position of the TRGB on the luminosity functions, and a horizontal dashed line indicates this location on the CMD. This line does not extend for the full width of the CMD to allow the reader to make an independent judgement of the location of the TRGB.

The output of our secondary, heuristic TRGB-finding technique is shown in the lower right panel. This method involves taking the ratio of the star counts in neighbouring bins from the luminosity histogram once the counts have passed a threshold level (see Paper I). Each bin is averaged with its immediate neighbours to attempt to reduce Poisson noise effects. This technique provides a 'sanity check' of our data-adaptive slope technique and should be in reasonable agreement with the more involved method. However, this technique has all the usual problems associated with edge-detection algorithms discussed previously, albeit this time in the log domain. This, coupled with the local neighbourhood averaging, leads to a tendency for this heuristic method to peak at systematically fainter magnitudes than the data-adaptive slope method, although the simplicity of the technique makes it attractive as a first pass on the data.

3.1 M31, the Andromeda galaxy

M31($0^{\mathrm{h}}\,42^{\mathrm{m}}\,44\overset{\mathrm{s}}{.}3$, $+41°\,16'\,9''$) is the closest giant spiral galaxy to the Milky Way. It provides a unique opportunity to study in detail a galaxy that is thought to be similar to our own. All the stellar populations that one would expect to find in a large disc galaxy

can be found in M31, and a detailed discussion of this vast and spectacular object is well beyond the scope of this paper.

Ferguson et al. (2002) and Irwin et al. (in preparation) present maps of the spatial distribution of red giant branch stars as seen in our INT WFC survey of this galaxy. Large amounts of substructure are obvious. However, we need to ensure that our distance estimate to this galaxy is unbiased by these features. For this reason, our analysis uses only those stars that are located within an elliptical annulus, $e = 0.4$, centred on M31, with a semimajor axis ranging from $2\overset{\circ}{.}25$ to $2\overset{\circ}{.}5$ ($\sim$35–40 kpc). This 'halo' zone is far enough from the centre of M31 to be not significantly affected by crowding or serious contamination from disc and/or bulge components. As the substructure revealed in our survey is spatially distinct its contribution within this annulus is small compared to the generic M31 halo population. We use as a reference field stars located in a similar, more distant, elliptical annulus with a semimajor axis ranging from $2\overset{\circ}{.}5$ to $2\overset{\circ}{.}8$.

The CMD and RGB luminosity functions for M31 are shown in Fig. 1. These are constructed from the elliptical annuli described above using all objects that lie within 3σ of the stellar locus, maximizing the number of stars available to us at this galactocentric radius. The TRGB is very obvious in these diagrams, and the TRGB algorithm applied to the LPD gives the results detailed below. Note that the metallicity used to calculate M_I^{TRGB} for this galaxy is not the median metallicity of the RGB but the representative metallicity of the strip of stars shown in the left panel of Fig. 1 ([M/H] ~ -1). Discussion of this result, and the following results, will be deferred until Section 4.

M31:

$$I_{\mathrm{TRGB}} = 20.54 \pm 0.03 \text{ mag}$$
$$E(B-V) = 0.06 \text{ mag}$$
$$[\mathrm{M/H}]_{\alpha=0.0} = -0.6$$
$$[\mathrm{M/H}]_{\alpha=0.3} = -0.5$$
$$M_I^{\mathrm{TRGB}} = -4.05 \text{ mag}$$
$$(m-M)_{\mathrm{o}} = 24.47 \pm 0.07 \text{ mag}$$
$$D_{\mathrm{M31}} = 785 \pm 25 \text{ kpc}$$

M31 error budget:

Photometry – rms	:	± 0.03 mag
– zero-point	:	± 0.02 mag
Reddening	:	± 0.02 mag
M_I^{TRGB}	:	± 0.05 mag
Algorithm	:	± 0.03 mag
Total	:	± 0.07 mag

3.2 NGC 205

NGC205($0^{\mathrm{h}}\,40^{\mathrm{m}}\,22\overset{\mathrm{s}}{.}1$, $+41°\,41'\,7''$), along with NGC 185 and 147, is one of three dwarf elliptical companions to M31. It lies only 37 arcmin ($\simeq$9 kpc) in projection from Andromeda and shows evidence of tidal interaction with its massive companion (e.g. Hodge 1973; Choi, Guhathakurta & Johnston 2002; McConnachie et al. 2004b). Multicolour photometry of the inner regions of this galaxy by Lee (1996) revealed a blue plume of stars and a bright asymptotic giant branch (AGB) population, indicating that both a young and intermediate age population are present. Earlier work by Mould, Kristian & Da Costa (1984) had shown that its metallicity was of order [Fe/H] $\simeq -0.9$, with a dispersion of $\sim$0.5.

NGC 205 falls well within the area surveyed as part of our INT WFC survey of M31, and one of our camera pointings is centred on this field. However, the centre of this field is unsuitable for direct analysis due to severe crowding and also significant contamination
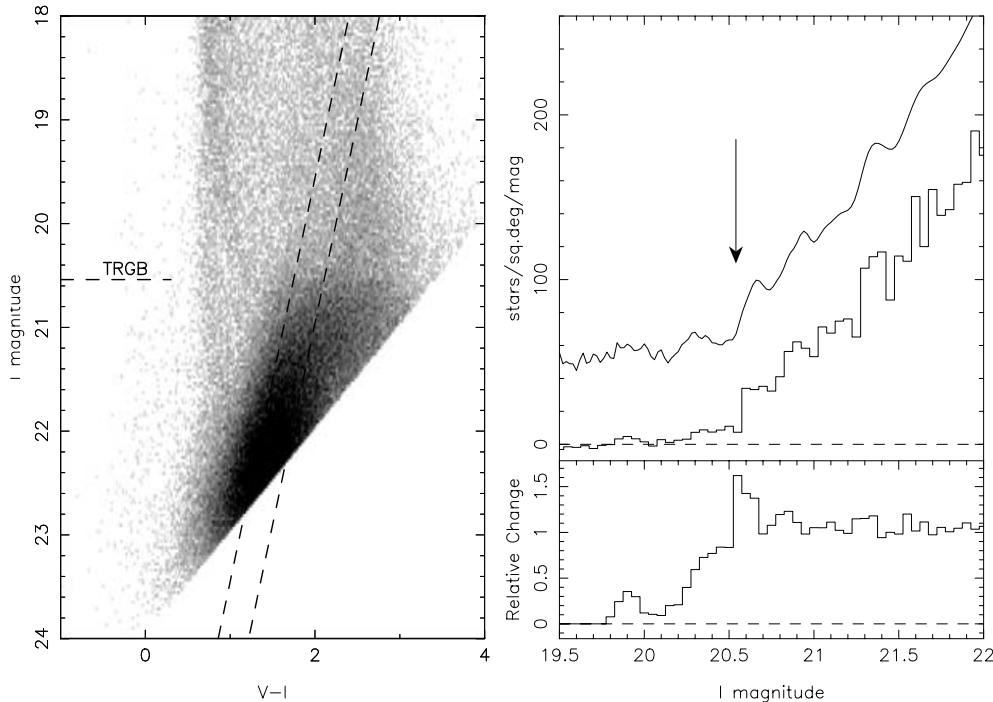
Figure 1. Hess diagram with square-root scaling showing the M31 CMD (left panel), RGB luminosity function and offset LPD (upper right panel), and heuristic signal (lower right panel). The TRGB is measured to lie at $I = 20.54$ mag and is marked on the CMD by a horizontal dashed line and on the luminosity functions by an arrow: stars within an elliptical annulus of $e = 0.4$ centred on M31, with a semimajor axis ranging from $2°\!\!.25$ to $2°\!\!.5$, were used in our analysis. Stars in an annulus outside of this were used as a reference field to correct for the foreground population.

from M31. Instead we use the neighbouring INT WFC field, further out on the M31 minor axis, which still contains a strong NGC 205 population but with much less crowding and a much weaker M31 population. Our reference field is the neighbouring field to this one, again further out on the minor axis. The resulting CMD and RGB luminosity functions for NGC 205 are shown in Fig. 2 and are constructed from objects lying within 2σ of the stellar locus in both filters. The TRGB is obvious in these diagrams, and application of our algorithm yields the following results. The group of stars immediately brighter than the tip, visible in the RGB luminosity function, is most likely a combination of bright AGB and M31 contamination. Note that the metallicity used to calculate M_I^{TRGB} for this galaxy is again not the median metallicity of the RGB but the representative metallicity of the strip of stars shown in the left panel of Fig. 2 ([M/H] ~ -1).

NGC 205:

$$I_{\mathrm{TRGB}} = 20.65 \pm 0.03 \,\mathrm{mag}$$
$$E(B - V) = 0.062 \,\mathrm{mag}$$
$$[\mathrm{M/H}]_{\alpha=0.0} = -0.8$$
$$[\mathrm{M/H}]_{\alpha=0.3} = -0.7$$
$$M_I^{\mathrm{TRGB}} = -4.05 \,\mathrm{mag}$$
$$(m - M)_0 = 24.58 \pm 0.07 \,\mathrm{mag}$$
$$D_{\mathrm{NGC205}} = 824 \pm 27 \,\mathrm{kpc}$$

NGC 205 error budget:

Photometry – rms	:	± 0.03 mag
– zero-point	:	± 0.02 mag
Reddening	:	± 0.02 mag
M_I^{TRGB}	:	± 0.05 mag
Algorithm	:	± 0.03 mag
Total	:	± 0.07 mag

3.3 NGC 185

NGC 185($0^{\mathrm{h}}\,38^{\mathrm{m}}\,58^{\mathrm{s}}\!.0$, $+48°\,20'\,15''$) is another dwarf elliptical companion to M31. Lee, Freedman & Madore (1993a) found strong evidence for three distinct stellar populations: a well-defined RGB, indicating a mean metallicity of [Fe/H] $= -1.23 \pm 0.16$, with a large dispersion; a bright AGB population above the TRGB, implying the presence of a strong intermediate age population; and some young stars with blue–yellow colours, suggesting that NGC 185 has Population I stars as well as Population II (see also Hodge 1963, 1973; Gallagher & Hunter 1981; Johnson & Gottesman 1983; Wiklind & Rydbeck 1986).

The CMD and RGB luminosity functions displayed in Fig. 3 are constructed from all the stars located further than $0°\!\!.1$ from the centre of NGC 185, but interior to $0°\!\!.2$. By only sampling stars in a ring around NGC 185, we negate the possible effects of crowding in the inner regions while still leaving a large enough area to act as a reference field. The lack of stars at magnitudes brighter than 20.2 in the resultant RGB luminosity function/LPD shows that the foreground is well removed by this technique. Additionally, due to the large number of objects for which we have good photometry, we have used only objects that lie within 2σ of the stellar locus in both filters. Application of our TRGB algorithm to the LPD for NGC 185 gives the results detailed below, along with the error budget for this galaxy. The value of the reddening from Schlegel et al. (1998) agrees well with that derived independently by Lee et al. (1993a) of $E(B - V) = 0.19 \pm 0.03$ mag.

NGC 185:

$$I_{\mathrm{TRGB}} = 20.23 \pm 0.03 \,\mathrm{mag}$$
$$E(B - V) = 0.179 \,\mathrm{mag}$$
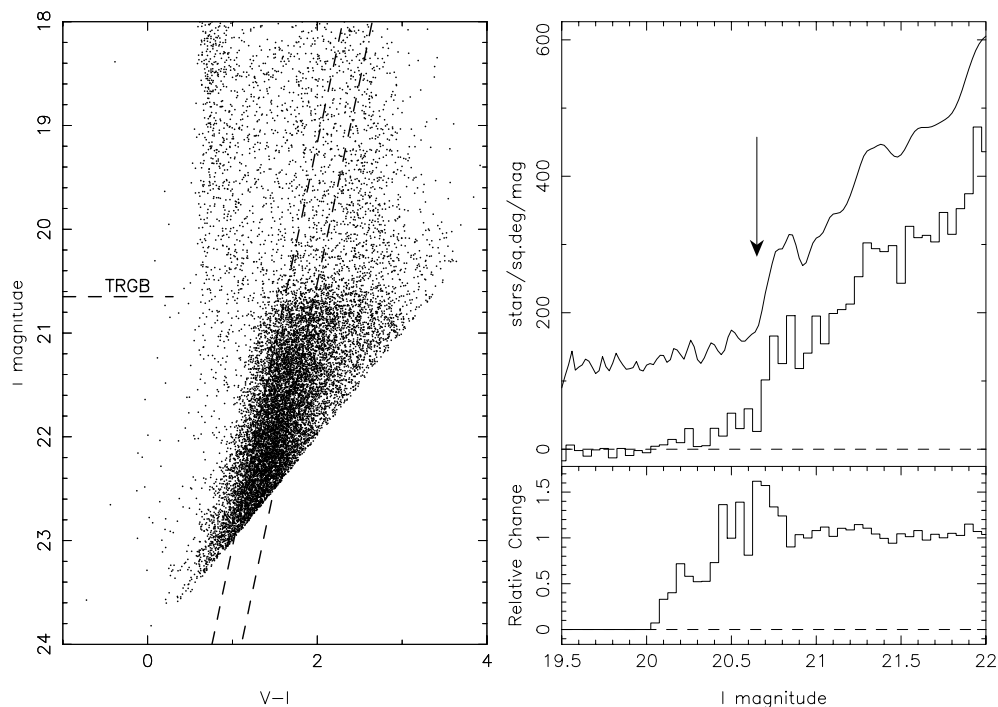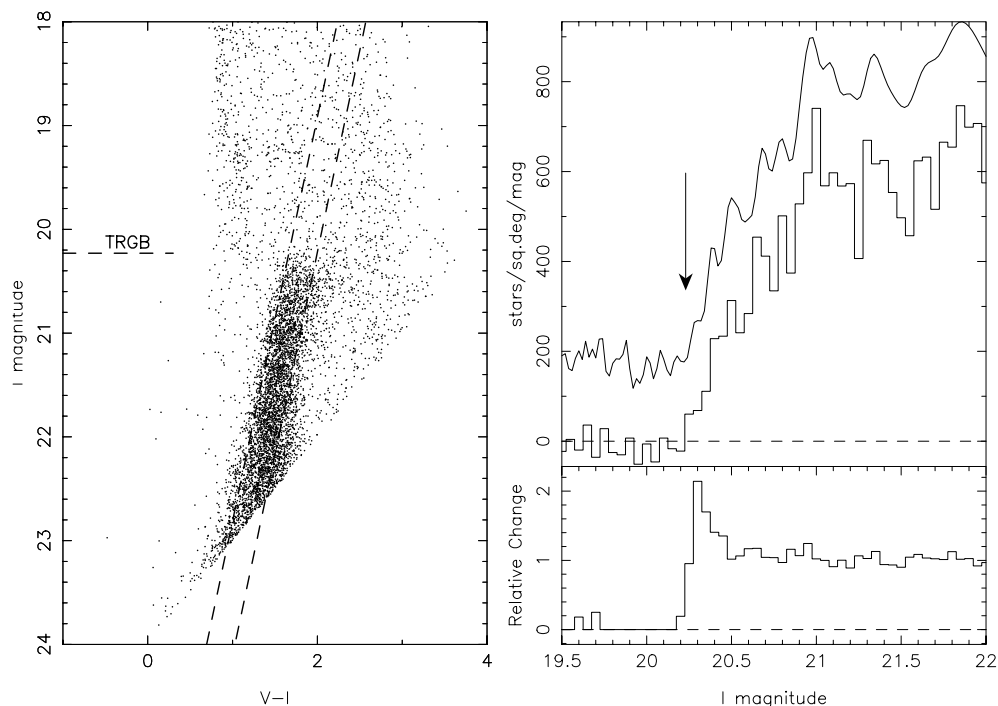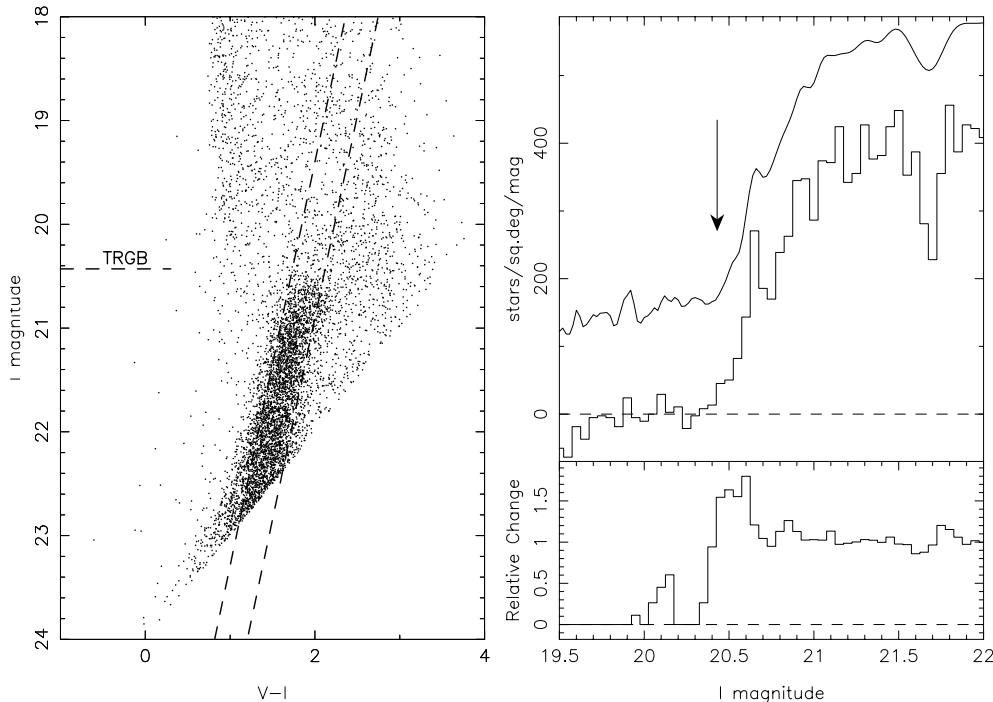$$[\mathrm{M/H}]_{\alpha=0.0} = -1.2$$

Figure 2. NGC 205 CMD (left panel), RGB luminosity function and offset LPD (upper right panel), and heuristic signal (lower right panel). The TRGB is measured to lie at $I = 20.65$ mag and is marked on the CMD by a horizontal dashed line and on the luminosity functions by an arrow.

Figure 3. NGC 185 CMD (left panel), RGB luminosity function and offset LPD (upper right panel), and heuristic signal (lower right panel). The TRGB is measured to lie at $I = 20.23$ mag and is marked on the CMD by a horizontal dashed line and on the luminosity functions by an arrow.

$$[M/H]_{\alpha=0.3} = -1.1$$
$$M_I^{TRGB} = -4.065 \text{ mag}$$
$$(m - M)_o = 23.95 \pm 0.09 \text{ mag}$$
$$D_{NGC185} = 616 \pm 26 \text{ kpc}$$

NGC 185 error budget:
    Photometry – rms : ±0.02 mag
        – zero-point : ±0.02 mag
    Reddening : ±0.06 mag

Figure 4. NGC 147 CMD (left panel), RGB luminosity function and offset LPD (upper right panel), and heuristic signal (lower right panel). The TRGB is measured to lie at $I = 20.43$ mag and is marked on the CMD by a horizontal dashed line and on the luminosity functions by an arrow.

M_I^{TRGB} : ± 0.05 mag
Algorithm : ± 0.03 mag
Total : ± 0.09 mag

3.4 NGC 147

NGC 147($0^{\mathrm{h}}\ 33^{\mathrm{m}}\ 12\overset{s}{.}1$, $+48°\ 30'\ 32''$) is another dwarf elliptical companions to M31, and it is recognized as being the most unique in terms of its stellar content. Han et al. (1997) conducted a thorough study of its stellar populations using the Wide Field Planetary Camera (WFPC2) on the *Hubble Space Telescope* (*HST*). The colour of the RGB implied a metallicity of [Fe/H] $\simeq -0.9$ although radial variations were observed in the average RGB colour and dispersion. Unlike NGC 185 and 205, no evidence for Population I stars was found, although an intermediate age population was observed.

The CMD and RGB luminosity functions shown in Fig. 4 are constructed from all the stars located exterior to $0\overset{\circ}{.}15$ from the centre of NGC 147, but within $0\overset{\circ}{.}25$. In a similar way to NGC 185, this helps negate the possible effects of crowding on our measurement. Due to the number of objects with good photometry, we use only objects lying within 2σ of the stellar locus. Inspection of the RGB luminosity function/LPD shows that the foreground is minimal. The result of the application of our TRGB algorithm to the LPD for NGC 147, and the error budget for this galaxy, is shown below.

NGC 147:

$I_{\mathrm{TRGB}} = 20.43 \pm 0.04$ mag
$E(B - V) = 0.175$ mag
$[\mathrm{M/H}]_{\alpha=0.0} = -1.1$
$[\mathrm{M/H}]_{\alpha=0.3} = -1.0$
$M_I^{\mathrm{TRGB}} = -4.055$ mag
$(m - M)_{\mathrm{o}} = 24.15 \pm 0.09$ mag
$D_{\mathrm{NGC147}} = 675 \pm 27$ kpc

NGC 147 error budget:
Photometry – rms : ± 0.02 mag
– zero-point : ± 0.02 mag
Reddening : ± 0.05 mag
M_I^{TRGB} : ± 0.05 mag
Algorithm : ± 0.04 mag
Total : ± 0.09 mag

3.5 Pegasus (DDO 216, UGC 12613)

Pegasus ($23^{\mathrm{h}}\ 28^{\mathrm{m}}\ 36\overset{s}{.}2$, $+14°\ 44'\ 35''$), unlike the previous systems, is a small dwarf irregular galaxy, discovered in the late 1950s by Wilson (Holmberg 1958). Hoessel & Mould (1982) were the first to study it in detail after the introduction of CCDs to astronomy; they found a lack of any bright young stars but did infer the presence of an old and intermediate stellar population from the presence of three red star clusters. More recently, Gallagher et al. (1998) have used WFPC2 in conjunction with ground-based data to study this galaxy. Their results show an object that has a surprising mix of stellar populations for such a small galaxy and suggest that Pegasus consists predominantly of a young-to-intermediate age population. This does not affect our use of the TRGB as a distance indicator for this galaxy, as the TRGB is of roughly constant magnitude for RGB stars older than 2 Gyr.

The CMD and RGB luminosity functions for Pegasus are shown in Fig. 5. These were constructed by using objects lying within 3σ of the stellar locus in both filters, located within $0\overset{\circ}{.}25$ of the centre of Pegasus. To negate possible crowding effects, we do not use the inner $0\overset{\circ}{.}05$. The onset of the RGB is evident at ~ 20.9 mag. The excess of stars brighter than this, visible in the RGB luminosity function/LPD, is attributed to an AGB population. The result of the application of our TRGB algorithm is detailed below.
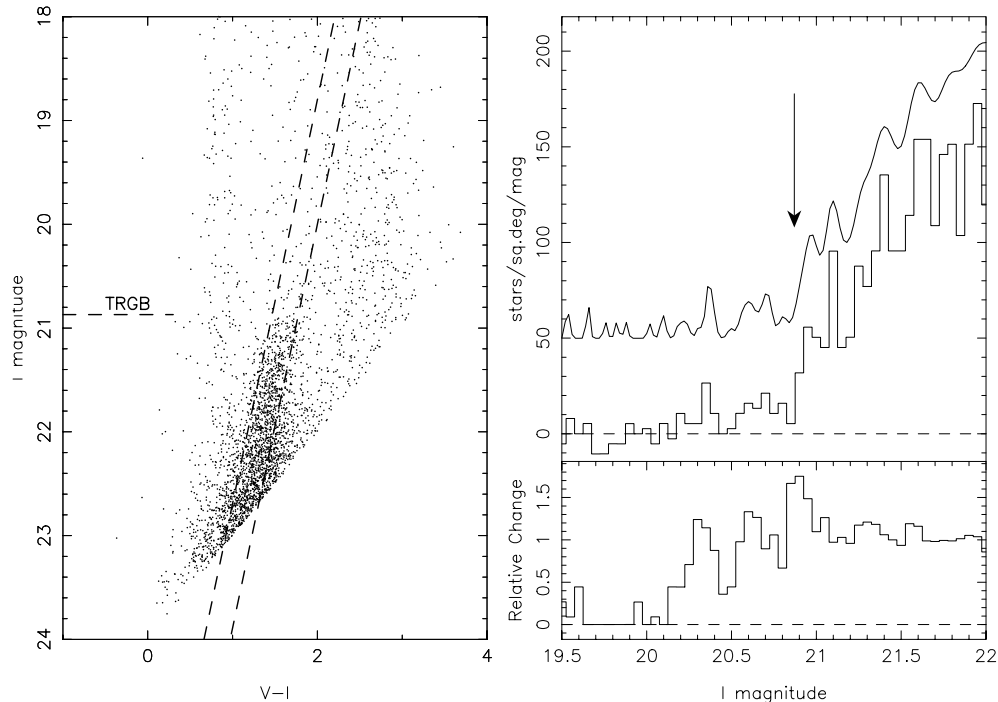
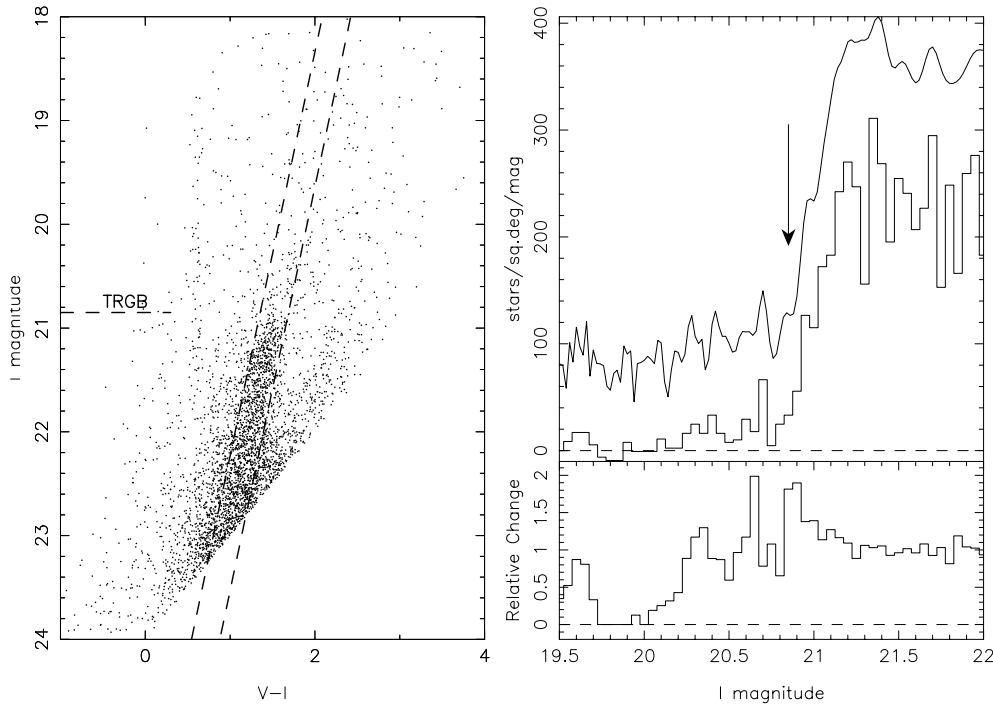**Figure 5.** Pegasus CMD (left panel), RGB luminosity function and offset LPD (upper right panel), and heuristic signal (lower right panel). The TRGB is measured to lie at $I = 20.87$ mag and is marked on the CMD by a horizontal dashed line and on the luminosity functions by an arrow.

Pegasus:

$$I_{\mathrm{TRGB}} = 20.87 \pm 0.03 \text{ mag}$$
$$E(B - V) = 0.064 \text{ mag}$$
$$[\mathrm{M/H}]_{\alpha=0.0} = -1.4$$
$$[\mathrm{M/H}]_{\alpha=0.3} = -1.2$$
$$M_I^{\mathrm{TRGB}} = -4.07 \text{ mag}$$
$$(m - M)_{\mathrm{o}} = 24.82 \pm 0.07 \text{ mag}$$
$$D_{\mathrm{Pegasus}} = 919 \pm 30 \text{ kpc}$$

Pegasus error budget:

Photometry – rms	:	± 0.03 mag
– zero-point	:	± 0.02 mag
Reddening	:	± 0.02 mag
M_I^{TRGB}	:	± 0.05 mag
Algorithm	:	± 0.03 mag
Total	:	± 0.07 mag

3.6 WLM (DDO 221)

WLM (Wolf–Lundmark–Melotte), located at $0^{\mathrm{h}} 1^{\mathrm{m}} 58\overset{\text{s}}{.}1$, $-15° 27' 39''$, is a dwarf irregular galaxy, discovered at the start of the twentieth century by Wolf (1910). In recent decades, several groups have analysed the stellar content of this object (Sandage & Carlson 1985; Ferraro et al. 1989; Minniti & Zijlstra 1997; Rejkuba et al. 2000). Minniti & Zijlstra (1997) derive a mean metallicity of $[\mathrm{Fe/H}] = -1.45 \pm 0.2$ from the colour of the RGB, and show that young and intermediate age stellar populations are present. The discovery of blue horizontal branch (HB) stars by Rejkuba et al. (2000) is an unambiguous indicator of an old stellar population. H II regions, Cepheids and planetary nebulae have also been detected (Sandage & Carlson 1985; Skillman, Terlevich & Melnick 1989; Jacoby & Lesser 1981) and it would seem that WLM consists of a disc-like component with possibly an old extended stellar halo.

Fig. 6 shows the CMD and RGB luminosity functions for WLM. These were constructed from all stars located within $0\overset{\circ}{.}2$ from the centre of this galaxy. Again, stars within $0\overset{\circ}{.}05$ of the centre were not used, to minimize potential problems due to crowding. The RGB is clearly visible in the CMD and an extended AGB also appears to be present. This is most clearly visible in the RGB luminosity function/LPD. The location of the tip, as derived by our algorithm, is detailed below. The slightly larger error on this measurement is due to the TRGB not being as clearly defined as in the previous examples, as inspection of the CMD shows.

WLM:

$$I_{\mathrm{TRGB}} = 20.85 \pm 0.05 \text{ mag}$$
$$E(B - V) = 0.035 \text{ mag}$$
$$[\mathrm{M/H}]_{\alpha=0.0} = -1.5$$
$$[\mathrm{M/H}]_{\alpha=0.3} = -1.4$$
$$M_I^{\mathrm{TRGB}} = -4.065 \text{ mag}$$
$$(m - M)_{\mathrm{o}} = 24.85 \pm 0.08 \text{ mag}$$
$$D_{\mathrm{WLM}} = 932 \pm 33 \text{ kpc}$$

WLM error budget:

Photometry – rms	:	± 0.02 mag
– zero-point	:	± 0.02 mag
Reddening	:	± 0.01 mag
M_I^{TRGB}	:	± 0.05 mag
Algorithm	:	± 0.05 mag
Total	:	± 0.08 mag

3.7 LGS3 (Pisces Dwarf)

LGS3($1^{\mathrm{h}} 3^{\mathrm{m}} 52\overset{\text{s}}{.}9$, $+21° 53' 05''$) is a very faint member of the Local Group, originally discovered by Karachentseva (1976) (see
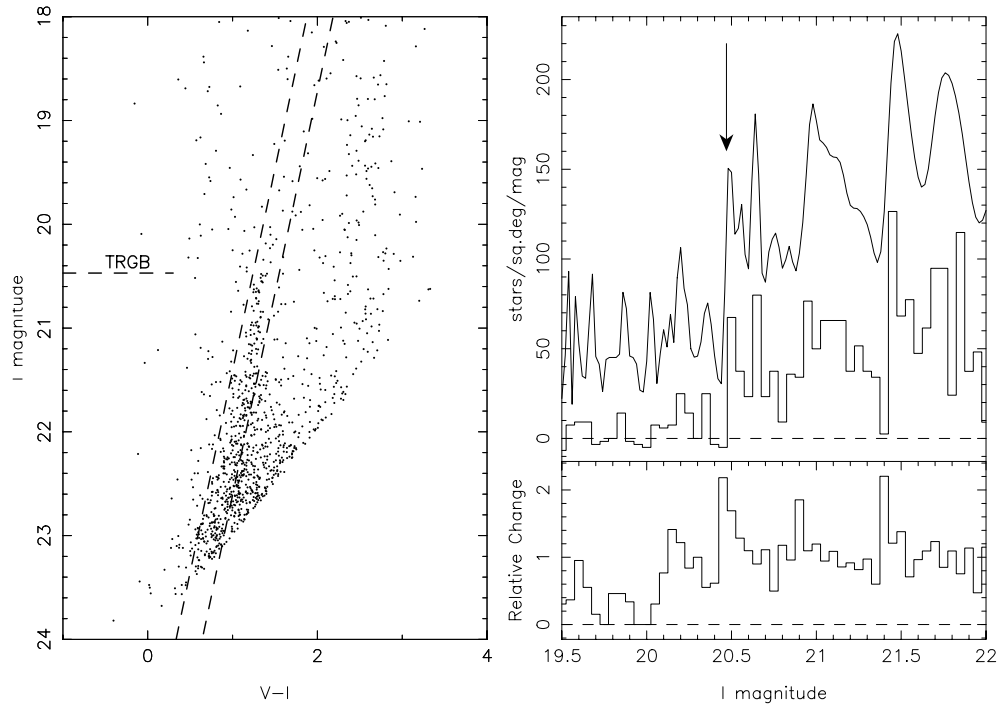
Figure 6. WLM CMD (left panel), RGB luminosity function and offset LPD (upper right panel), and heuristic signal (lower right panel). The TRGB is measured to lie at $I = 20.85$ mag and is marked on the CMD by a horizontal dashed line and on the luminosity functions by an arrow.

also Kowal, Lo & Sargent 1978; Thuan & Martin 1979). Lee (1995) conducted a study of the stellar populations; an RGB is evident and its colour implies a metallicity of $[Fe/H] = -2.10 \pm 0.22$. A small number of bright AGB stars and several blue stars are also observed. Along with the Phoenix dwarf galaxy, LGS3 is suspected of being a transition-type galaxy, somewhere between a dwarf irregular and a dwarf spheroidal galaxy (Cook & Olszewski 1989; van de Rydt, Demers & Kunkel 1991). It could be that this is a real transition object, but the possibility that it is merely a rare, but statistically acceptable, version of one of the two classes must also be considered (see Lee 1995 and Aparicio, Gallart & Bertelli 1997 for differing conclusions on this matter).

The CMD and RGB luminosity functions for LGS3 are shown in Fig. 7. They have been constructed from all stellar objects located within $0°.15$ of the centre of this galaxy. LGS3 is a much fainter galaxy than the previous ones and so its CMD is much more sparsely populated. As such, its RGB luminosity function/LPD is relatively noisy. A large increase in the number of stars is readily observable, however, at ~ 20.5 mag which we attribute to the TRGB. Below are the results from the application of our algorithm. We have been unable to calculate the full MDF for LGS3 because a large fraction of the stars in LGS3 appear at least as metal-poor as our most metal-poor evolutionary tracks. We therefore adopt this as the typical metallicity of the system.

LGS3:

$$I_{TRGB} = 20.47 \pm 0.03 \text{ mag}$$
$$E(B - V) = 0.042 \text{ mag}$$
$$[M/H]_{\alpha=0.0} \lesssim -2.3$$
$$[M/H]_{\alpha=0.3} \lesssim -2.0$$
$$M_I^{TRGB} = -4.04 \text{ mag}$$
$$(m - M)_o = 24.43 \pm 0.07 \text{ mag}$$
$$D_{LGS3} = 769 \pm 23 \text{ kpc}$$

LGS3 error budget:

$$\text{Photometry – rms} : \pm 0.02 \text{ mag}$$
$$\text{– zero-point} : \pm 0.02 \text{ mag}$$
$$\text{Reddening} : \pm 0.01 \text{ mag}$$
$$M_I^{TRGB} : \pm 0.05 \text{ mag}$$
$$\text{Algorithm} : \pm 0.03 \text{ mag}$$
$$\text{Total} : \pm 0.07 \text{ mag}$$

3.8 Cetus

Cetus (0^h 26^m 11^s, $-11°$ $2'$ $40''$) was only recently discovered by Whiting, Hau & Irwin (1999) as part of the same survey that also led to the discovery of a Local Group galaxy in Antlia (Whiting, Irwin & Hau 1997). Sarajedini et al. (2002) have conducted a survey of the stellar populations of this dwarf spheroidal using the WFPC2 instrument on the *HST*. The colour of the RGB suggests a metallicity of $[Fe/H] = -1.7$, with a dispersion of $\simeq 0.2$. A strong red HB is observed with indications of a less numerous bluer component. The HB is observed to be significantly redder than those for globular clusters of similar metallicities. They conclude that this is a manifestation of the second-parameter effect, and if it is accepted that this is due to age, then Cetus is 2–3 Gyr younger than these globular clusters.

The CMD and RGB luminosity function for Cetus is shown in Fig. 8. This has been constructed from all stellar objects located within $0°.2$ from the centre of this galaxy, and the onset of the RGB can be clearly seen. Application of our algorithm to the LPD yields the results presented below.

Cetus:

$$I_{TRGB} = 20.39 \pm 0.03 \text{ mag}$$
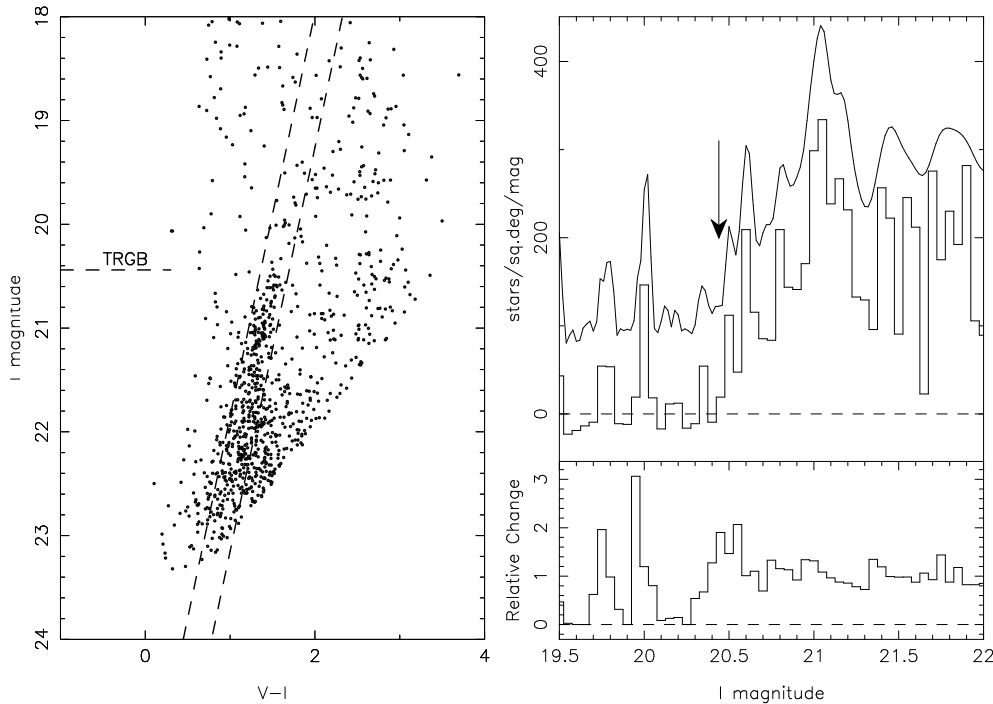$$E(B - V) = 0.029 \text{ mag}$$
$$[M/H]_{\alpha=0.0} = -1.6$$

Figure 7. LGS3 CMD (left panel), RGB luminosity function and offset LPD (upper right panel), and heuristic signal (lower right panel). The TRGB is measured to lie at $I = 20.47$ mag and is marked on the CMD by a horizontal dashed line and on the luminosity functions by an arrow.
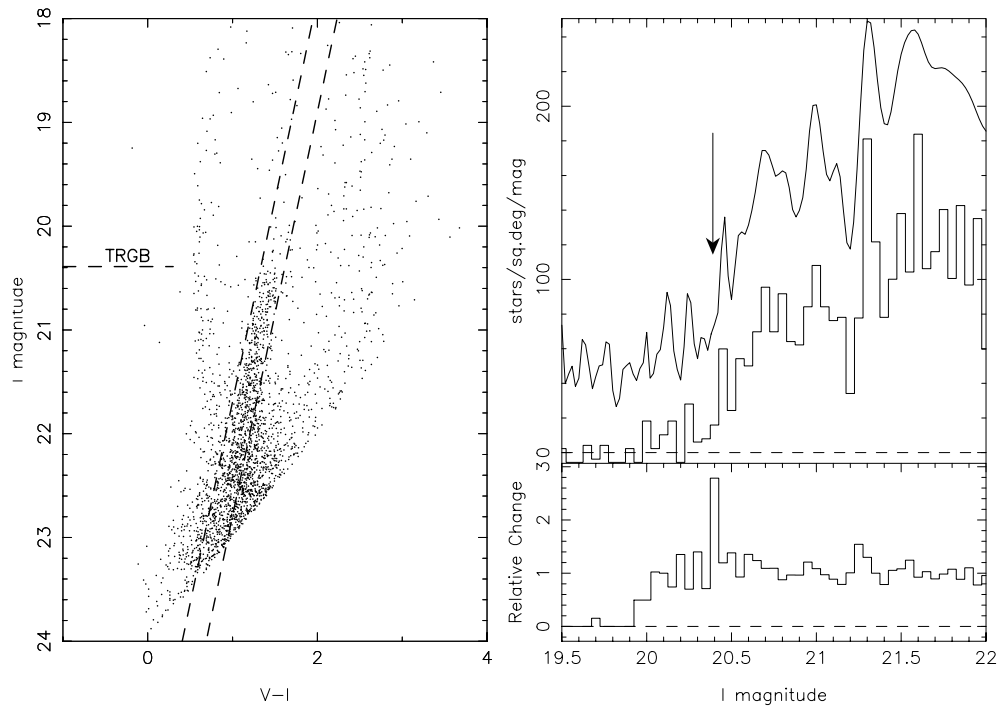
Figure 8. Cetus CMD (left panel), RGB luminosity function and offset LPD (upper right panel), and heuristic signal (lower right panel). The TRGB is measured to lie at $I = 20.39$ mag and is marked on the CMD by a horizontal dashed line and on the luminosity functions by an arrow.

$$[M/H]_{\alpha=0.3} = -1.5$$
$$M_I^{TRGB} = -4.055 \text{ mag}$$
$$(m - M)_o = 24.39 \pm 0.07 \text{ mag}$$
$$D_{Cetus} = 755 \pm 23 \text{ kpc}$$

Cetus error budget:
  Photometry – rms : ± 0.02 mag

  – zero-point : ± 0.02 mag
  Reddening : ± 0.01 mag
  M_I^{TRGB} : ± 0.05 mag
  Algorithm : ± 0.03 mag
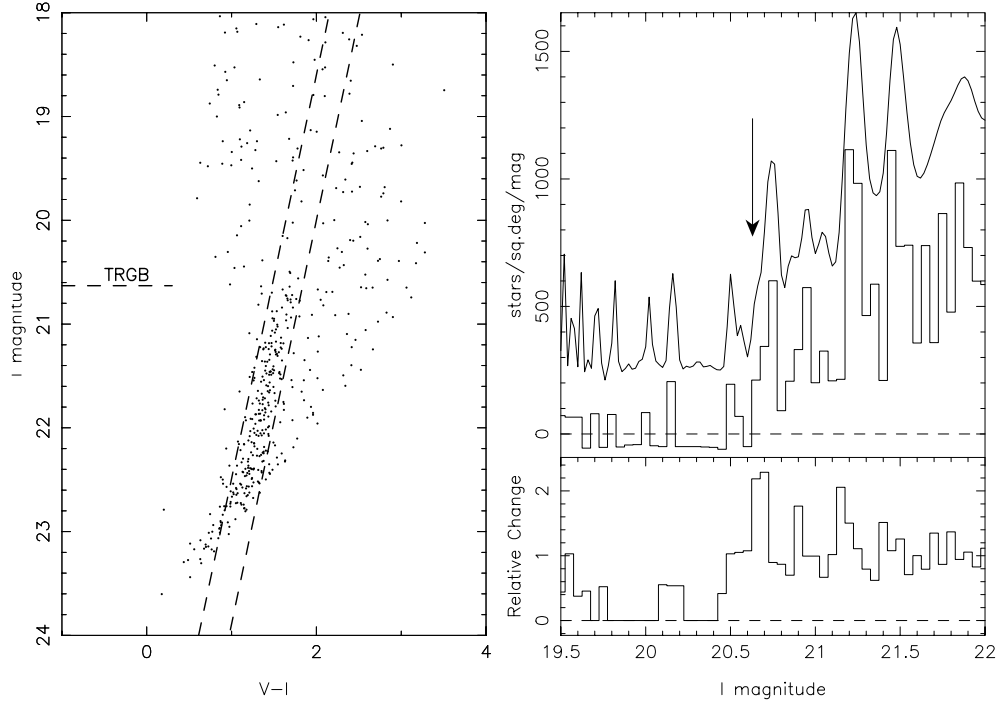 Total : ± 0.07 mag

Figure 9. And III CMD (left panel), RGB luminosity function and offset LPD (upper right panel), and heuristic signal (lower right panel). The TRGB is measured to lie at $I = 20.44$ mag and is marked on the CMD by a horizontal dashed line and on the luminosity functions by an arrow.

3.9 Andromeda III

The Andromeda III dwarf spheroidal galaxy ($0^h 35^m 33^s.8$, $+36° 29' 52''$) was discovered by van den Bergh 1972b (see also van den Bergh 1972a) along with Andromeda I and II, and the background dwarf irregular Andromeda IV. Da Costa, Armandroff & Caldwell (2002) have used WFPC2 to obtain deep photometry as part of their *HST* survey of the stellar populations of the dwarf spheroidal satellites of M31 (Da Costa et al. 1996, 2000). By comparing the RGB with those of standard globular clusters, And III is found to have a mean metallicity of [Fe/H] $\simeq -1.88$ and a dispersion of 0.12 (see also Armandroff et al. 1993). It has a very obvious HB, which is in fact redder than that in both And I and II. Since it is also metal-poorer than both these systems, then this is interpreted as being due to age effects. If correct, And III must therefore be younger than the globular clusters by $\sim$3 Gyr. The interested reader is referred to fig. 10 in Da Costa et al. (2002) which has an excellent comparison of their deep CMDs for And I, II and III.

Fig. 9 shows the CMD and RGB luminosity function for all stellar objects within $0°.1$ of the centre of And III. A smaller area is used so as to detect more clearly the RGB over and above the foreground stars. The CMD and RGB luminosity functions are slightly noisy due to the faintness of the galaxy, although the onset of the TRGB is readily visible in the RGB luminosity function/LPD. Application of our TRGB algorithm yields the results detailed below.

And III:

$$I_{\text{TRGB}} = 20.44 \pm 0.04 \text{ mag}$$
$$E(B - V) = 0.058 \text{ mag}$$
$$[\text{M/H}]_{\alpha=0.0} = -1.7$$
$$[\text{M/H}]_{\alpha=0.3} = -1.6$$
$$M_I^{\text{TRGB}} = -4.045 \text{ mag}$$
$$(m - M)_o = 24.37 \pm 0.07 \text{ mag}$$
$$D_{\text{AndIII}} = 749 \pm 24 \text{ kpc}$$

And III error budget:

Photometry – rms :	± 0.02 mag
– zero-point :	± 0.02 mag
Reddening :	± 0.02 mag
M_I^{TRGB} :	± 0.05 mag
Algorithm :	± 0.04 mag
Total :	± 0.07 mag

3.10 Andromeda V, Andromeda VI (Pegasus dSph) and Andromeda VII (Cassiopeia dSph)

Andromeda V ($1^h 10^m 17^s.1$, $+47° 37' 41''$), VI ($23^h 51^m 46^s.3$, $+24° 34' 57''$) and VII ($23^h 26^m 31^s, +50° 41' 31''$) were, prior to the discovery of And IX, the three newest additions to the M31 subgroup. And V and VI were discovered by Armandroff et al. (1998, 1999) after they had performed an analysis on the digitized version of the second Palomar Sky Survey (POSS-II; Reid et al. 1991; Lasker & Postman 1993; Reid & Djorgovski 1993). At the same time, Karachentsev & Karachentseva (1999) independently discovered And V (which they named the Pegasus dSph) as well as yet another companion, the Cassiopeia dSph (also named And VII) from their analysis of the POSS-II plates. All of these satellites appear to resemble typical dwarf spheroidals, with little or no evidence for young or intermediate stellar populations (Armandroff et al. 1998, 1999; Grebel & Guhathakurta 1999; Hopp et al. 1999; Davidge et al. 2002). Their metallicities, as derived from the colour of their RGBs, are [Fe/H] $\simeq -1.3$ for And VI (Grebel & Guhathakurta 1999), and [Fe/H] $\simeq -1.4$ for And VII. And V was originally measured to have a metallicity of [Fe/H] $\simeq -1.5$ by Armandroff et al. (1998), but a more recent measurement by Davidge et al. (2002) measures this object as being significantly more metal-poor, at [Fe/H] $= -2.2 \pm 0.1$. The more recent measurement places this object firmly on the

Figure 10. And V CMD (left panel), RGB luminosity function and offset LPD (upper right panel), and heuristic signal (lower right panel). The TRGB is measured to lie at $I = 20.63$ mag and is marked on the CMD by a horizontal dashed line and on the luminosity functions by an arrow.

expected relation between integrated luminosity and metallicity for dwarf spheroidal galaxies (e.g. see fig. 4 of Caldwell 1999).

Stars within $0°05 (\simeq 2.5 r_c$; Caldwell 1999) of the centre of And V are used to construct the CMD and RGB luminosity functions shown in Fig. 10. The result of the application of our algorithm to the LPD is detailed below.

And V:

$$I_{TRGB} = 20.63 \pm 0.04 \text{ mag}$$
$$E(B - V) = 0.124 \text{ mag}$$
$$[M/H]_{\alpha=0.0} = -1.6$$
$$[M/H]_{\alpha=0.3} = -1.5$$
$$M_I^{TRGB} = -4.055 \text{ mag}$$
$$(m - M)_o = 24.44 \pm 0.08 \text{ mag}$$
$$D_{AndV} = 774 \pm 28 \text{ kpc}$$

And V error budget:

Photometry – rms	: ±0.02 mag
– zero-point	: ±0.02 mag
Reddening	: ±0.04 mag
M_I^{TRGB}	: ±0.05 mag
Algorithm	: ±0.04 mag
Total	: ±0.08 mag

The CMD and RGB luminosity function for all the stars located within $0°05$ from the centre of And VI is shown in Fig. 11. The result of the application of our algorithm to the LPD is detailed below; the few stars in the luminosity functions immediately brighter than the tip can be seen to be unassociated with the RGB by inspection of the CMD. It may be that these stars are foreground contamination or some extended AGB component.

And VI:

$$I_{TRGB} = 20.53 \pm 0.04 \text{ mag}$$
$$E(B - V) = 0.065 \text{ mag}$$

$$[M/H]_{\alpha=0.0} = -1.5$$
$$[M/H]_{\alpha=0.3} = -1.3$$
$$M_I^{TRGB} = -4.065 \text{ mag}$$
$$(m - M)_o = 24.47 \pm 0.07 \text{ mag}$$
$$D_{AndVI} = 783 \pm 25 \text{ kpc}$$

And VI error budget:

Photometry – rms	: ±0.02 mag
– zero-point	: ±0.02 mag
Reddening	: ±0.02 mag
M_I^{TRGB}	: ±0.05 mag
Algorithm	: ±0.04 mag
Total	: ±0.07 mag

Fig. 12 shows the CMD and RGB luminosity function for And VII. These are constructed from all stars within $0°15$ from the centre of this galaxy. The result of the TRGB algorithm is shown below. The grouping of stars brighter than the proposed tip location are most likely an AGB population; inspection of the CMD shows that this grouping is unlikely to be associated with the TRGB.

And VII:

$$I_{TRGB} = 20.73 \pm 0.05 \text{ mag}$$
$$E(B - V) = 0.199 \text{ mag}$$
$$[M/H]_{\alpha=0.0} = -1.4$$
$$[M/H]_{\alpha=0.3} = -1.3$$
$$M_I^{TRGB} = -4.07 \text{ mag}$$
$$(m - M)_o = 24.41 \pm 0.10 \text{ mag}$$
$$D_{AndVII} = 763 \pm 35 \text{ kpc}$$

And VII error budget:

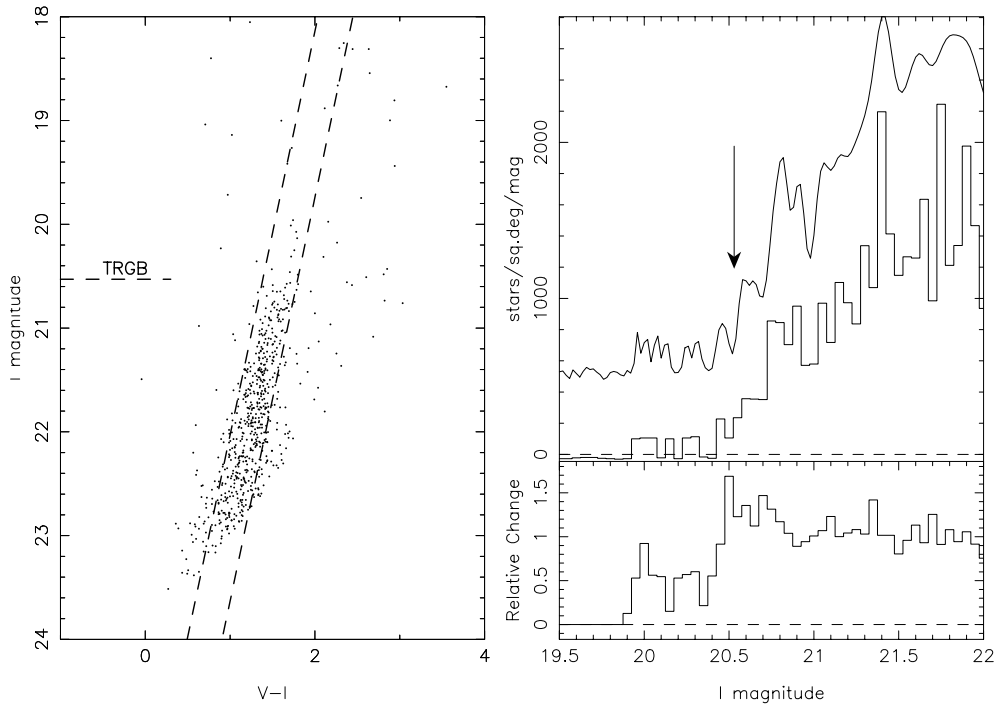|	
Photometry – rms	: ±0.03 mag
– zero-point	: ±0.02 mag
Reddening	: ±0.06 mag
M_I^{TRGB}	: ±0.05 mag

Figure 11. And VI CMD (left panel), RGB luminosity function and offset LPD (upper right panel), and heuristic signal (lower right panel). The TRGB is measured to lie at $I = 20.53$ mag and is marked on the CMD by a horizontal dashed line and on the luminosity functions by an arrow.
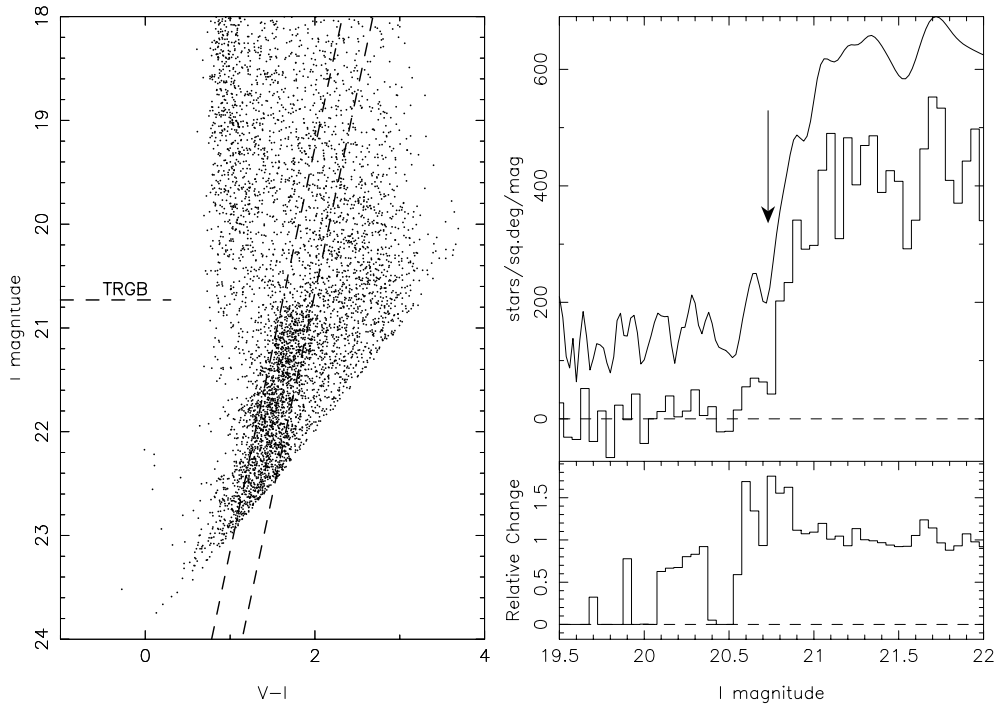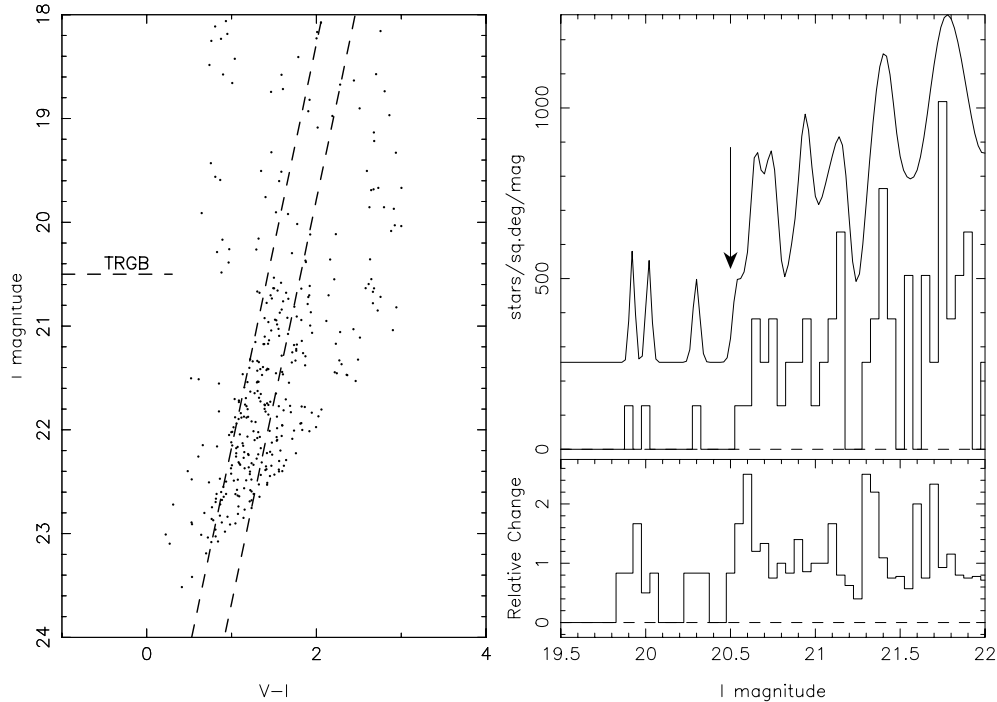

Figure 12. And VII CMD (left panel), RGB luminosity function and offset LPD (upper right panel), and heuristic signal (lower right panel). The TRGB is measured to lie at $I = 20.73$ mag and is marked on the CMD by a horizontal dashed line and on the luminosity functions by an arrow.

Algorithm : ± 0.05 mag
Total : ± 0.10 mag

3.11 Andromeda IX

Andromeda IX ($0^h 52^m 52\overset{s}{.}8$, $+43° 12' 0''$) was only very recently discovered by Zucker et al. (2004) during inspection of an SDSS

scan of the environs of M31. It is the faintest galaxy so far discovered, with a surface brightness of $\Sigma_V \simeq 26.8$ mag arcsec^{-2} and appears to be very similar in morphological properties to the other dwarf spheroidal companions of M31. Due to its recent discovery, detailed information about its stellar content has not yet been obtained.

The CMD and RGB luminosity function for And IX is shown in Fig. 13. These are constructed from all stars within $0\overset{\circ}{.}05$ from

Figure 13. And IX CMD (left panel), RGB luminosity function and offset LPD (upper right panel), and heuristic signal (lower right panel). The TRGB is measured to lie at $I = 20.50$ mag and is marked on the CMD by a horizontal dashed line and on the luminosity functions by an arrow.

the centre of this galaxy. There is an apparent lack of foreground contamination present in this field due to its small size, and comparison of the And IX CMD with a reference CMD offset 10 arcmin to the north-west shows there are virtually no M31 field stars in the region of the TRGB of And IX. As such, subtraction of a reference field from the And IX luminosity function does not alter our result. The onset of the TRGB in this galaxy is clear, and the result of the application of our TRGB algorithm is shown below.

And IX:

$$I_{\mathrm{TRGB}} = 20.50 \pm 0.03 \text{ mag}$$
$$E(B - V) = 0.077 \text{ mag}$$
$$[\mathrm{M/H}]_{\alpha=0.0} = -1.5$$
$$[\mathrm{M/H}]_{\alpha=0.3} = -1.4$$
$$M_I^{\mathrm{TRGB}} = -4.065 \text{ mag}$$
$$(m - M)_0 = 24.42 \pm 0.07 \text{ mag}$$
$$D_{\mathrm{AndIX}} = 765 \pm 24 \text{ kpc}$$

And IX error budget:

Photometry – rms	:	± 0.02 mag
– zero-point	:	± 0.02 mag
Reddening	:	± 0.02 mag
M_I^{TRGB}	:	± 0.05 mag
Algorithm	:	± 0.03 mag
Total	:	± 0.07 mag

3.12 Aquarius (DDO 210)

Aquarius is located at $20^{\mathrm{h}} 46^{\mathrm{m}} 51\overset{\mathrm{s}}{.}8, \ -12^{\circ} 50' 53''$ and is generally considered to be located at the periphery of the Local Group. Discovered in the late 1950s by van den Bergh (1959), an in-depth study of its stellar population has recently been conducted by Lee et al. (1999). This author found that the galaxy is relatively metal-

poor, at $[\mathrm{Fe/H}] \simeq -1.86$. The central regions have recently seen enhanced star formation, and several young stars are observed. An RGB and AGB are also seen, indicating the presence of intermediate and old stellar populations, as would be expected for a dwarf irregular galaxy. Overall, there appears to be some evidence for a disc–halo split in the stellar content, similar to WLM, although this has yet to be confirmed by other observations.

The CMD and RGB luminosity functions for Aquarius are presented in Fig. 14, constructed from the innermost $0\overset{\circ}{.}075$ of this galaxy. In addition to the RGB, a blue plume of stars is also observed, demonstrating the existence of a population of young stars, in agreement with Lee et al. (1999). As inspection of Fig. 14 shows, this is the hardest galaxy in our sample on which to perform our analysis. The difficulty is due to the feature located between $I \sim 20.5$ and 21.2 mag. This relatively bright excess could be the onset of the RGB of Aquarius, a bright AGB population, or a foreground population. We rule out the latter option as this feature seems to be robust against any spatial cuts and foreground corrections that we choose to apply. Without more information it is difficult to distinguish between the two remaining possibilities. Our preferred interpretation is that it is a bright AGB population; Lee et al. (1999) have shown that we would expect to see such a feature. The fainter excess at $I > 21.2$ mag appears much more populated and well-defined than the proposed AGB feature, and so we interpret this as the RGB population. Under this hypothesis, the TRGB algorithm produces the results detailed below. Additionally, as was the case for LGS3, a large fraction of the stars in Aquarius appear as metal-poor as our most metal poor evolutionary track. This has therefore been adopted as the typical metallicity of this system.

Aquarius:

$$I_{\mathrm{TRGB}} = 21.21 \pm 0.04 \text{ mag}$$
$$E(B - V) = 0.052 \text{ mag}$$
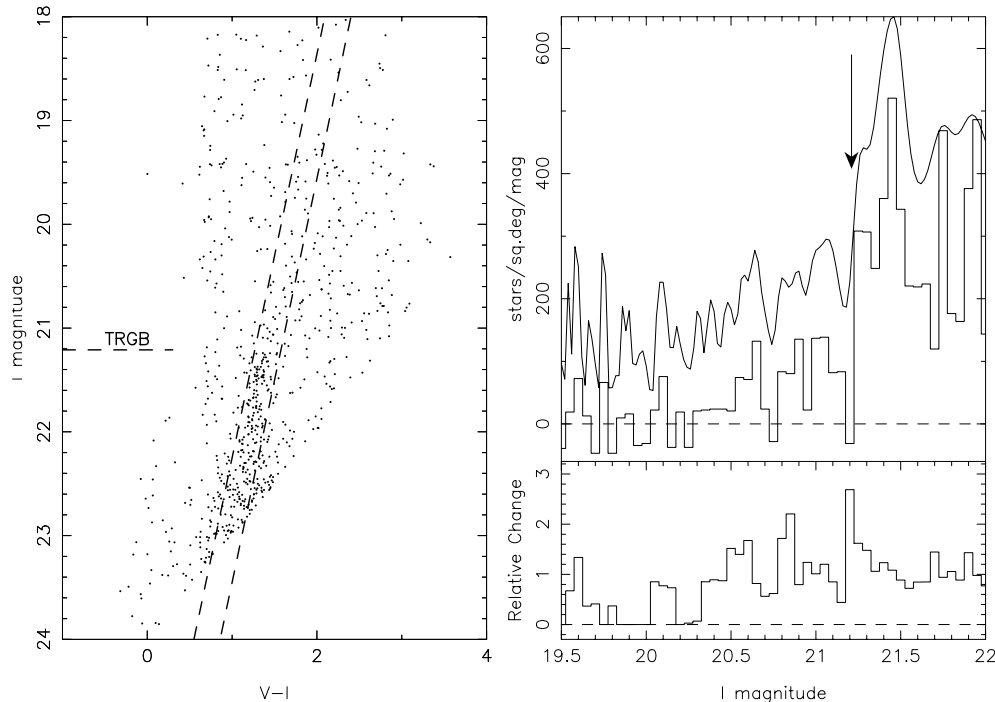$$[\mathrm{M/H}]_{\alpha=0.0} \lesssim -2.3$$

Figure 14. Aquarius CMD (left panel), RGB luminosity function and offset LPD (upper right panel), and heuristic signal (lower right panel). The TRGB is measured to lie at $I = 21.21$ mag and is marked on the CMD by a horizontal dashed line and on the luminosity functions by an arrow.

$$[M/H]_{\alpha=0.3} \lesssim -2.0$$
$$M_I^{TRGB} = -4.04 \text{ mag}$$
$$(m - M)_o = 25.15 \pm 0.08 \text{ mag}$$
$$D_{Aquarius} = 1071 \pm 39 \text{ kpc}$$

Aquarius error budget:

Photometry – rms	:	± 0.04 mag
– zero-point	:	± 0.02 mag
Reddening	:	± 0.02 mag
M_I^{TRGB}	:	± 0.05 mag
Algorithm	:	± 0.04 mag
Total	:	± 0.08 mag

4 SUMMARY

Table 1 lists the galaxies analysed as part of this study, including those from Paper I, along with their positions, the adopted values for the reddening, the median metallicities as determined by the colour of the red giant branch and the adopted value of M_I^{TRGB} using the modified calibration of Bellazzini et al. (2004). Table 2 list the measured position of the TRGB, the distance modulus and distance for each galaxy. The three galaxies originally analysed in Paper I have had their distances recalculated to correct for the slight metallicity dependency that was not previously addressed in Paper I. Additionally, the TRGB location in M33 has been rederived using a local foreground correction (in the same way as for M31) and using only objects that lie within 2σ of the stellar locus. Also included for comparison is a selection of previous distance estimates to each system from the literature. Fig. 15 shows a graphical comparison between our results and these earlier measurements. In general, good agreement is observed and no obvious systematic offsets or trends are visible. For those cases where Cepheid distances are available

(M31: Freedman & Madore 1990; Joshi et al. 2003; M33: Lee et al. 2002) our results match these estimates to within better than a few tens of kiloparsecs.

For a few of the fainter objects in our sample (e.g. And IX) we have relatively few bright RGB stars available to us, due to the lack of such stars in these systems. The distance measurements implicitly assume that the brightest RGB stars in the system are good indicators of the actual position of the TRGB. For the case of And IX, the RGB luminosity function shows a steep rise and is clearly defined, compensating in part for the fewer stars available to us. Thus relatively accurate TRGB measurements can be obtained for these systems, even though the number of bright RGB stars is far less than, say, NGC 205 or M31.

We conclude with a list of some of the main results evident from this study.

(i) The distance to the newly discovered dwarf spheroidal companion to M31, Andromeda IX, is measured to be 765 ± 25 kpc. This is in good agreement with the distance calculated by Zucker et al. (2004). Assuming And IX does not have a strong α-element enhancement, its metallicity is measured to be [Fe/H] $\simeq -1.5$. Fig. 4 of Caldwell (1999) shows an empirical relation that is found to exist between integrated luminosity and metallicity for dwarf spheroidal galaxies, such that fainter galaxies have lower metallicity. Zucker et al. (2004) measure $M_{tot,V} \simeq -8.3$ mag which would imply that And IX should have a metallicity of approximately [Fe/H] ~ -2.2. And IX thus appears to be more metal-rich than this empirical relation would suggest.

(ii) And V is measured to have [Fe/H]$= -1.6$, again assuming no α-enhancement. This disagrees with the recent measurement by Davidge et al. (2002) of [Fe/H] $= -2.2$. It does agree, however, with the earlier measurement by Armandroff et al. (1998). Both this latter measurement and our measurement indicate that, like And IX, And V does not lie on the
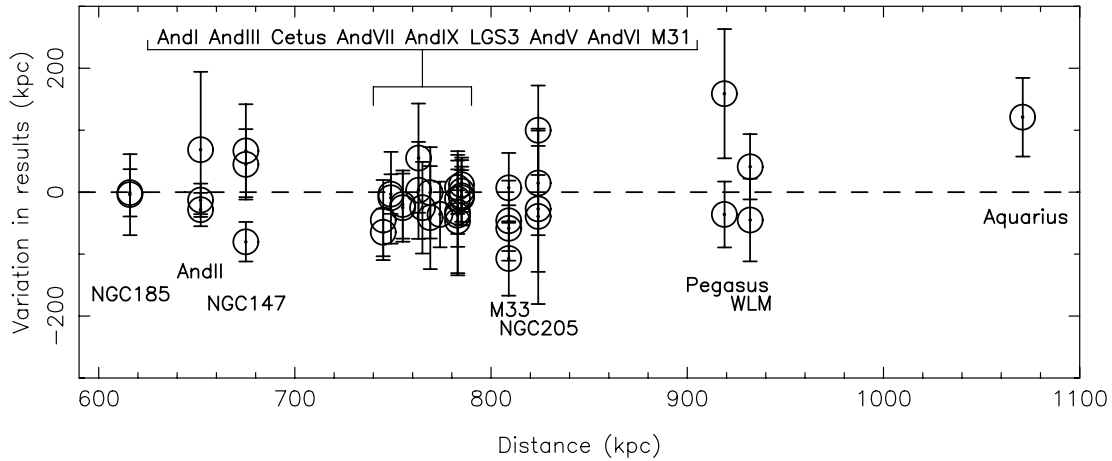
Figure 15. The distances we derive for the galaxies listed in Table 2 compared to the selection of previous estimates also listed in that table. The *x*-axis is the distance we derive; the *y*-axis is the difference between our result and the previous estimates, such that points lying below the dashed line are previous estimates that are larger than those presented here. Given the spread in distance values for any given galaxy and the relatively large error bars, there are no obvious biases or trends in our distance estimates. In general, they are seen to be in good agreement with previous work.

expected relation between integrated luminosity and metallicity. These results suggest that And I, II, III, V, VI, VII and IX all have comparable metallicities in the range $-1.7 \leqslant$ [Fe/H] $\leqslant$ 1.4, with an estimated accuracy on the measurements of $\pm \sim 0.1 - 0.2$ dex.

(iii) Aquarius is confirmed to lie ~ 1 Mpc from the Milky Way. Early estimates of its distance had placed it well outside the zero-velocity surface of the Local Group until Lee et al. (1999) showed that it was substantially closer than this. We note, however, that the distance to Aquarius is the least certain from this study for the reasons discussed in Section 3.12. It could potentially lie closer to us than we have derived here.

(iv) Pegasus is measured to lie at 919 ± 30 kpc. This measurement agrees with earlier work done by Aparicio (1994). A more recent study by Gallagher et al. (1998) places this object some 160 kpc closer – this distance is required by their study so as to fit self-consistent stellar population models based upon the Geneva stellar evolutionary tracks. Gallagher et al. (1998) also require to adopt a larger reddenning value than is normally assumed for Pegasus $[E(B - V) \simeq 0.14]$ in order to match the colours of the main sequence. Even by adopting this larger reddening value, the TRGB distance appears incompatible with their measurement of the distance.

(v) NGC 185 and 147 have previously been suspected of forming a binary system due to their small angular separation ($\sim 1°$) and similar line of sight distances (van den Bergh 1998). The distances that we derive for these objects suggest that they are likely to be gravitationally bound, separated in line of sight by only ~ 60 kpc. One degree at the distance of this system corresponds to ~ 11 kpc, and so their physical separation is also of order 60 kpc, although the uncertainties in each of their distances means that the precise value may be substantially different from this.

The 17 Local Group galaxies listed in Tables 1 and 2 were observed with the same telescope, instrument and filters for similar exposure times and the resulting data were reduced using the same pipeline processing. An identical analysis was then conducted on each to calculate the position of the TRGB, its median metallicity and its distance. The use of a Wide Field Camera has maximized the number of stars observed per pointing. This reduces the effect of Poisson noise on our measurements and ensures that the luminosity

function that we derive is as accurate a representation of the intrinsic luminosity function of the galaxy as is possible in the region of the tip. The resulting set of metallicity and distance estimates has thus had systematic uncertainties minimized and are therefore ideal for any study of Local Group galaxy properties.

REFERENCES

Aparicio A., 1994, ApJ, 437, L27
Aparicio A., Gallart C., Bertelli G., 1997, AJ, 114, 680
Arce H. G., Goodman A. A., 1999, ApJ, 512, L135
Armandroff T. E., Da Costa G. S., Caldwell N., Seitzer P., 1993, AJ, 106, 986
Armandroff T. E., Davies J. E., Jacoby G. H., 1998, AJ, 116, 2287
Armandroff T. E., Jacoby G. H., Davies J. E., 1999, AJ, 118, 1220
Barker M. K., Sarajedini A., Harris J., 2004, ApJ, 606, 869
Bellazzini M., Ferraro F. R., Pancino E., 2001, ApJ, 556, 635
Bellazzini M., Cacciari C., Federici L., Fusi Pecci F., Rich M., 2003, A&A, 405, 867
Bellazzini M., Ferraro F. R., Sollima A., Pancino E., Origlia L., 2004, A&A, 424, 199
Bonifacio P., Monai S., Beers T. C., 2000, AJ, 120, 2065
Brown T. M., Ferguson H. C., Smith E., Kimble R. A., Sweigart A. V., Renzini A., Rich R. M., 2004, AJ, 127, 2738
Caldwell N., 1999, AJ, 118, 1230

Choi P. I., Guhathakurta P., Johnston K. V., 2002, AJ, 124, 310
Ciardullo R., Jacoby G. H., Ford H. C., Neill J. D., 1989, ApJ, 339, 53
Cook K. H., Olszewski E., 1989, BAAS, 21, 775
Da Costa G. S., Armandroff T. E., 1990, AJ, 100, 162
Da Costa G. S., Armandroff T. E., Caldwell N., Seitzer P., 2000, AJ, 119, 705
Da Costa G. S., Armandroff T. E., Caldwell N., Seitzer P., 1996, AJ, 112, 2576
Da Costa G. S., Armandroff T. E., Caldwell N., 2002, AJ, 124, 332
Davidge T. J., Da Costa G. S., Jørgensen I., Allington-Smith J. R., 2002, AJ, 124, 886
Durrell P. R., Harris W. E., Pritchet C. J., 2001, AJ, 121, 2557
Durrell P. R., Harris W. E., Pritchet C. J., 2004, AJ, 128, 260
Ferguson A. M. N., Irwin M. J., Ibata R. A., Lewis G. F., Tanvir N. R., 2002, AJ, 124, 1452
Ferraro F. R., Fusi Pecci F., Tosi M., Buonanno R., 1989, MNRAS, 241, 433
Freedman W. L., Madore B. F., 1990, ApJ, 365, 186
Gallagher J. S., Hunter D. A., 1981, AJ, 86, 1312
Gallagher J. S., Tolstoy E., Dohm-Palmer R. C., Skillman E. D., Cole A. A., Hoessel J. G., Saha A., Mateo M., 1998, AJ, 115, 1869
Galleti S., Bellazzini M., Ferraro F. R., 2004, A&A, 423, 925
Grebel E. K., Guhathakurta P., 1999, ApJ, 511, L101
Greggio L., Marconi G., Tosi M., Focardi P., 1993, AJ, 105, 894
Han M., Hoessel J. G., Gallagher J. S., Holtsman J., Stetson P. B., 1997, AJ, 113, 1001
Hodge P. W., 1963, AJ, 68, 691
Hodge P. W., 1973, ApJ, 182, 671
Hoessel J. G., Mould J. R., 1982, ApJ, 254, 38
Holmberg E., 1958, Medd. Lunds Astron. Obs., Ser II, 128
Hopp U., Schulte-Ladbeck R. E., Greggio L., Mehlert D., 1999, A&A, 342, L9
Ibata R., Irwin M., Lewis G., Ferguson A. M. N., Tanvir N., 2001, Nat, 412, 49
Irwin M., Lewis J., 2001, New Astron. Rev., 45, 105
Irwin M. et al., 2004, in Quinn P. J., Bridger A., eds, Proc. SPIE Vol. 5493, Optimizing Scientific Return for Astronomy through Information Technologies. SPIE, Bellingham, WA, p. 411
Jacoby G. H., Lesser M. P., 1981, AJ, 86, 185
Johnson D. W., Gottesman S. T., 1983, ApJ, 275, 549
Joshi Y. C., Pandey A. K., Narasimha D., Sagar R., Giraud-Héraud Y., 2003, A&A, 402, 113
Karachentseva V. E., 1976, Comm. Special Obs., 18, 42
Karachentsev I. D., Karachentseva V. E., 1999, A&A, 341, 355
Kim M., Kim E., Lee M. G., Sarajedini A., Geisler D., 2002, AJ, 123, 244
Koenig C. H. B., Nemec J. M., Mould J. R., Fahlman G. G., 1993, AJ, 106, 1819
Kowal C. T., Lo K. Y., Sargent W. L. W., 1978, IAU Circ., 3305, 2
Landolt A. U., 1992, AJ, 104, 372
Lasker B. M., Postman M., 1993, in ASP Conf. Ser. Vol. 43, Sky Surveys. Protostars to Protogalaxies. Astron Soc. Pac., San Francisco, p. 131
Lee M. G., 1995, AJ, 110, 1129
Lee M. G., 1996, AJ, 112, 1438
Lee M. G., Freedman W. L., Madore B. F., 1993a, AJ, 106, 964
Lee M. G., Freedman W. L., Madore B. F., 1993b, ApJ, 417, 553
Lee M. G., Aparicio A., Tikonov N., Byun Y., Kim E., 1999, AJ, 118, 853
Lee M. G., Kim M., Sarajedini A., Geisler D., Gieren W., 2002, ApJ, 565, 959

Lynden-Bell D., 1999, in Whitelock P., Cannon R., eds, Proc. IAU Symp., The Stellar Content of Local Group Galaxies. Astron. Soc. Pac., San Francisco, p. 39
Méndez B., Davis M., Moustakas J., Newman J., Madore B. F., Freedman W. L., 2002, AJ, 124, 213
Martínez-Delgado D., Aparicio A., 1998, AJ, 115, 1462
McConnachie A. W., Irwin M. J., Ibata R. A., Ferguson A. M. N., Lewis G. F., Tanvir N., 2003, MNRAS, 343, 1335
McConnachie A. W., Irwin M. J., Ferguson A. M. N., Ibata R. A., Lewis G. F., Tanvir N., 2004a, MNRAS, 350, 243
McConnachie A. W., Irwin M. J., Lewis G. F., Ibata R. A., Chapman S. C., Ferguson A. M. N., Tanvir N. R., 2004b, MNRAS, 351, L94
Mateo M. L., 1998, ARA&A, 36, 435
Minniti D., Zijlstra A. A., 1997, AJ, 114, 147
Mould J., Kristian J., 1990, ApJ, 354, 438
Mould J. R., Kristian J., Da Costa G. S., 1983, ApJ, 270, 471
Mould J., Kristian J., Da Costa G. S., 1984, ApJ, 278, 575
Pritzl B. J., Armandroff T. E., Jacoby G. H., Da Costa G. S., 2002, AJ, 124, 1464
Pritzl B. J., Armandroff T. E., Jacoby G. H., Da Costa G. S., 2004, AJ, 127, 318
Reid N., Djorgovski S., 1993, in ASP Conf. Ser. Vol. 43, Sky Surveys. Protostars to Protogalaxies. Astron Soc. Pac., San Francisco, p. 125
Reid I. N. et al., 1991, PASP, 103, 661
Rejkuba M., Minniti D., Gregg M. D., Zijlstra A. A., Alonso M. V., Goudfrooij P., 2000, AJ, 120, 801
Saha A., Hoessel J. G., Mossman A. E., 1990, AJ, 100, 108
Saha A., Hoessel J. G., Krist J., 1992, AJ, 103, 84
Sakai S., Madore B. F., Freedman W. L., 1996, ApJ, 461, 713
Salaris M., Cassisi S., 1997, MNRAS, 289, 406
Salaris M., Cassisi S., 1998, MNRAS, 298, 166
Sandage A., Carlson G., 1985, AJ, 90, 1464
Sarajedini A. et al., 2002, ApJ, 567, 915
Schlegel D. J., Finkbeiner D. P., Davis M., 1998, ApJ, 500, 525
Skillman E. D., Terlevich R., Melnick J., 1989, MNRAS, 240, 563
Thompson I. B., Kaluzny J., Pych W., Burley G., Krzeminski W., Paczyński B., Persson S. E., Preston G. W., 2001, AJ, 121, 3089
Thuan T. X., Martin G. E., 1979, ApJ, 232, L11
Tiede G. P., Sarajedini A., Barker M. K., 2004, AJ, 128, 224
Tikhonov N. A., Karachentsev I. D., 1999, Astron. Lett., 25, 332
van de Rydt F., Demers S., Kunkel W. E., 1991, AJ, 102, 130
VandenBerg D. A., Swenson F. J., Rogers F. J., Iglesias C. A., Alexander D. R., 2000, ApJ, 532, 430
van den Bergh S., 1959, Publ. David Dunlop Obs., 2, 147
van den Bergh S., 1972a, ApJ, 178, L99
van den Bergh S., 1972b, ApJ, 171, L31
van den Bergh S., 1998, AJ, 116, 1688
van den Bergh S., 1999, A&A, 9, 273
Walton N. A., Lennon D. J., Greimel R., Irwin M. J., Lewis J. R., Rixon G. T., 2001, The Newsletter of the Isaac Newton Group of Telescopes (ING Newsl.), Issue No. 4, p. 7–8
Whiting A. B., Irwin M. J., Hau G. K. T., 1997, AJ, 114, 996
Whiting A. B., Hau G. K. T., Irwin M., 1999, AJ, 118, 2767
Wiklind T., Rydbeck G., 1986, A&A, 164, L22
Wolf M., 1910, Astron. Nachr., 183, 187
Zucker D. B. et al., 2004, ApJ, 612, L121

This paper has been typeset from a TEX/LATEX file prepared by the author.